nature ecology & evolution

Article

https://doi.org/10.1038/s41559-025-02891-5

A novel Hox gene promoter fuels the evolution of adaptive phenotypic plasticity in wing eyespots of satyrid butterflies

Received: 27 June 2025

Accepted: 1 October 2025

Published online: 24 October 2025

Check for updates

Shen Tian ✉, Bonnie Lee, Tirtha Das Banerjee, Suriya Narayanan Murugesan & Antónia Monteiro ✉

Adaptive phenotypic plasticity allows organisms to display distinct phenotypes in response to variable environments, but little is known about the genomic changes that promote the evolution of plasticity on a macroevolutionary scale. Here, combining tissue-specific transcriptomics, comparative genomics and genome editing, we show that temperature-mediated plasticity in the size of butterfly eyespot wing patterns, a derived seasonal adaptation estimated to have evolved ~60 million years ago at the base of the satyrid clade (~2,700 extant species), is fuelled by the recruitment of a Hox gene *Antennapedia* (*Antp*) to eyespot development. In satyrid butterflies, *Antp* regulates eyespot size in a temperature-dependent manner, increasing plasticity levels. The cooption of *Antp* to eyespots was driven by the evolution of a novel eyespot-specific promoter in satyrid genomes, which when disrupted in a model satyrid, *Bicyclus anynana*, reduced plasticity levels. We show that a taxon-specific cis-regulatory innovation in a conserved developmental gene fuelled the evolution of adaptive phenotypic plasticity across a large clade of animals.

Phenotypic plasticity describes the ability of organisms to use a single genotype to produce distinct phenotypes in response to environmental cues[1,2]. When these cues are sensed during development, plasticity can alter developmental trajectories to produce fitter phenotypes adapted to each environment[3]. Whereas we have an increasing body of knowledge how gene-regulatory patterns change in response to environments[4–6] or how genomic changes underly variations in plasticity levels within a species[7–10], we have a much fuzzier understanding of the genomic changes that alter an ancestral, non-plastic species into a clade of plastic species. Here we use recent technical and conceptual advances in a classic model system of adaptive phenotypic plasticity—plasticity in the size of eyespot wing colour pattern in satyrid butterflies—to explore the evolution of plasticity in a comparative phylogenetic framework.

The evolutionary origins and mechanisms of butterfly eyespot size plasticity have been primarily explored in *Bicyclus anynana* and its satyrid relatives. In *B. anynana*, ventral hindwing eyespot size increases with increasing environmental temperatures associated with the hot, wet season and decreases with cold, dry season temperatures in tropical Africa[11,12] (Fig. 1a). This temperature-mediated eyespot size plasticity helps individuals evade predators via different strategies in each season[13,14] and appears to be restricted to Satyrinae[15–18], a subfamily originated ~60 million years ago with ~2,700 species containing *B. anynana*[19,20]. In *B. anynana*, hindwing eyespot size plasticity is associated with, and partially regulated by, temperature-induced dynamics of an insect hormone 20-hydroxyecdysone (20E) during the larval–pupal transition[21–23] (Fig. 1b). However, comparative work showed that variation in the titres of this hormone with temperature, and expression of the hormone receptor (EcR) in eyespot central cells, are not sufficient to explain how satyrid butterflies evolved eyespot size plasticity[17]. It is, thus, still unclear how the common ancestor of satyrids including *B. anynana* evolved temperature-mediated eyespot size plasticity.

Department of Biological Sciences, Faculty of Science, National University of Singapore, Singapore, Singapore. ✉e-mail: shen.tian@u.nus.edu; antonia.monteiro@nus.edu.sg

https://doi.org/10.1038/s41559-025-02891-5

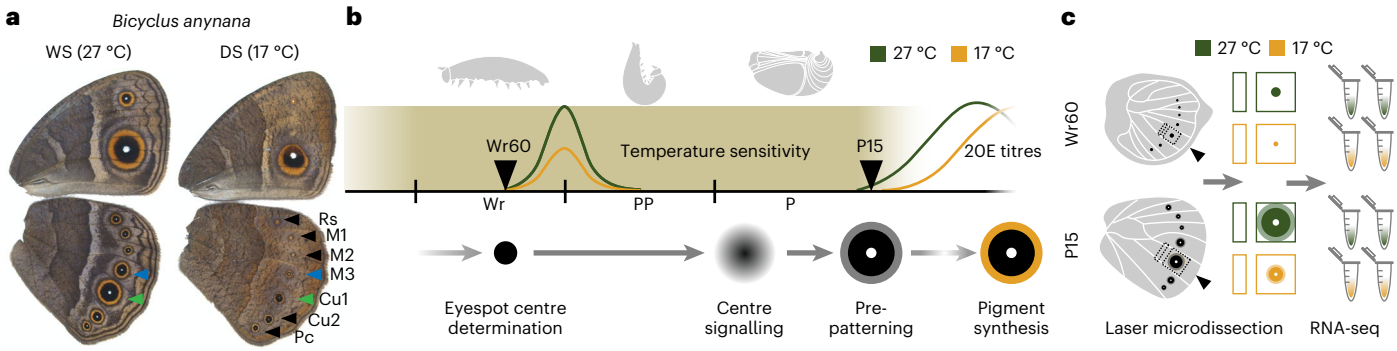

Fig. 1 | Tissue-specific transcriptomes generated from a developmental window of plasticity. a, The model satyrid *Bicyclus anynana* exhibits ventral hindwing eyespot size plasticity in response to rearing temperatures. WS, wet season; DS, dry season. Arrowheads denote hindwing sectors. **b**, New temperature-shift experiments revealed a developmental window (shaded area), when eyespot size is highly sensitive to rearing temperatures. The highly sensitive period covers essential eyespot developmental stages and temperature-induced dynamics of the insect hormone 20-hydroxyecdysone (20E), previously shown to be associated with the development of plasticity[21–23]. Green and orange curves depict wet- and dry-season 20E titres, respectively. **c**, Within the sensitive period, two time points, at 60% wanderer (Wr60) and 15% pupal (P15) stages, were chosen to generate tissue-specific transcriptomes across seasonal forms at each time point.

To elucidate the mechanistic evolution of eyespot size plasticity in Satyrinae, we first generated a tissue-specific transcriptomic atlas within a refined temperature-sensitive developmental window in the model satyrid *B. anynana*, aiming to resolve eyespot-specific correlates of molecular plasticity in response to temperature. From the transcriptome, we identified and functionally validated a Hox gene, *Antennapedia* (*Antp*), as a conserved regulator of satyrid eyespot size plasticity. We then investigated how *Antp* regulates plasticity in a trait- and taxon-specific manner, focusing on the conservation of sequences, activities and functions of alternative *Antp* promoters within and outside Satyrinae.

Tissue-specific transcriptomes during the development of plasticity

To resolve how external temperature cues shape internal molecular landscapes, it is essential to identify the key developmental window when eyespot size is most sensitive to rearing temperatures. Previous temperature-shift experiments suggested that eyespot size is most sensitive to temperatures experienced during the final fifth instar larval (L5) stage, especially the late wanderer (Wr) stage[23,24]. To confirm and improve and complement these results, we repeated these experiments with a refined design (Extended Data Fig. 1 and Supplementary Table 1) and found that the most temperature-sensitive developmental window is wider than previously proposed[23], spanning Wr, pre-pupal (PP) and the first 15% pupal (P15) stages—the larval–pupal transition (Fig. 1b, Extended Data Fig. 1 and Supplementary Text 1). This wider period overlaps critical eyespot developmental stages: around mid to late L5, when multiple transcription factors are expressed in the developing eyespot centre cells, and the period right after pupation to the end of P15, when eyespot centre cells signal to the surrounding cells (within 18 h post-pupation, 27 °C) and activate genes that pre-pattern the eyespot rings and thus the final eyespot size (~24 h post-pupation, 27 °C) (ref. 25) (Fig. 1b).

To construct tissue-specific transcriptomes, we focused on one larval time point, 60% of the wanderer stage (Wr60) and one pupal time point, P15, within the temperature-sensitive window (Fig. 1b). This strategy allowed us to capture both the early upstream regulators and the more downstream effectors of eyespot size. Tissue-specific transcriptomes were generated by laser microdissections of both the hindwing eyespot tissue from the Cu1 wing sector (Fig. 1a, green arrowheads, and Fig. 1c, black arrowheads) and an adjacent control wing tissue from the proximal side of the same sector, from both seasonal forms of *B. anynana* females, at each developmental time point (Fig. 1c).

Gene expression plasticity is largely systemic rather than trait specific

To evaluate the degree of trait-specific gene expression plasticity in response to temperature, we quantified gene expression across all samples (Supplementary Fig. 1) and investigated if plastic genes (differentially expressed across seasonal forms, adjusted p values (padj) < 0.05) in the eyespot tissue were also similarly plastic (in the same direction) in the control tissue—a systemic form of plasticity. We found that over half of the plastic genes in eyespots are systemic, whereas the rest show eyespot-specific plasticity (Fig. 2a, Supplementary Table 2 and Supplementary Text 2). Gene set enrichment analyses also suggested that most plastic genes in eyespots share functional terms with genes showing systemic plasticity (Supplementary Text 2). We hypothesized that genes with eyespot-specific plasticity or different plasticity levels across tissue types were more likely to mediate the development of trait-specific phenotypic plasticity, thus we focused on those genes for subsequent investigations.

For ease of picking candidate genes for experimental validation, we shortlisted genes showing eyespot-specific plasticity by selecting genes with high plasticity levels ($|\log_2$ fold change (FC)$|$ > 0.8) with high significance (padj < 0.01) and considerable expression levels in eyespots (mean transcript per million (TPM) > 2). This generated two shortlists of candidates at each period (Wr60: 54 genes; P15: 54 genes) (Fig. 2a and Supplementary Table 2). From the Wr60 list, of particular interest is *Antp*, a Hox gene essential in forewing eyespot development, but merely used to pattern the eyespot white centres and to increase eyespot size in hindwings[26]. Hybridization chain reaction (HCR) confirmed the eyespot-specific high expression of *Antp* in wet-season larval wings, as reported before[26]. Our transcriptomic data show that *Antp* exhibits eyespot-specific plasticity, with higher expression levels in wet-season, compared with dry-season eyespots during Wr60 (Fig. 2b). This plastic expression pattern was also confirmed at the protein level with immunostaining (Fig. 3).

From the two shortlists, we also picked candidates with unknown functions to visualize their spatial expression patterns using HCR and/or to test their roles using CRISPR-Cas9-mediated genome editing (Supplementary Figs. 2–4, Supplementary Tables 3–5 and Supplementary Text 3). We identified *bric à brac* (*bab*), a gene potentially required to specify brown background wing colour and define the outer boundary of the eyespot orange ring during P15 (Fig. 2b).

Outside the stringently filtered shortlists, we also performed HCR staining on *Optix* and *spalt* (*sal*), two known regulators of the eyespot orange ring and black disk[27], respectively, during P15 across seasonal

https://doi.org/10.1038/s41559-025-02891-5

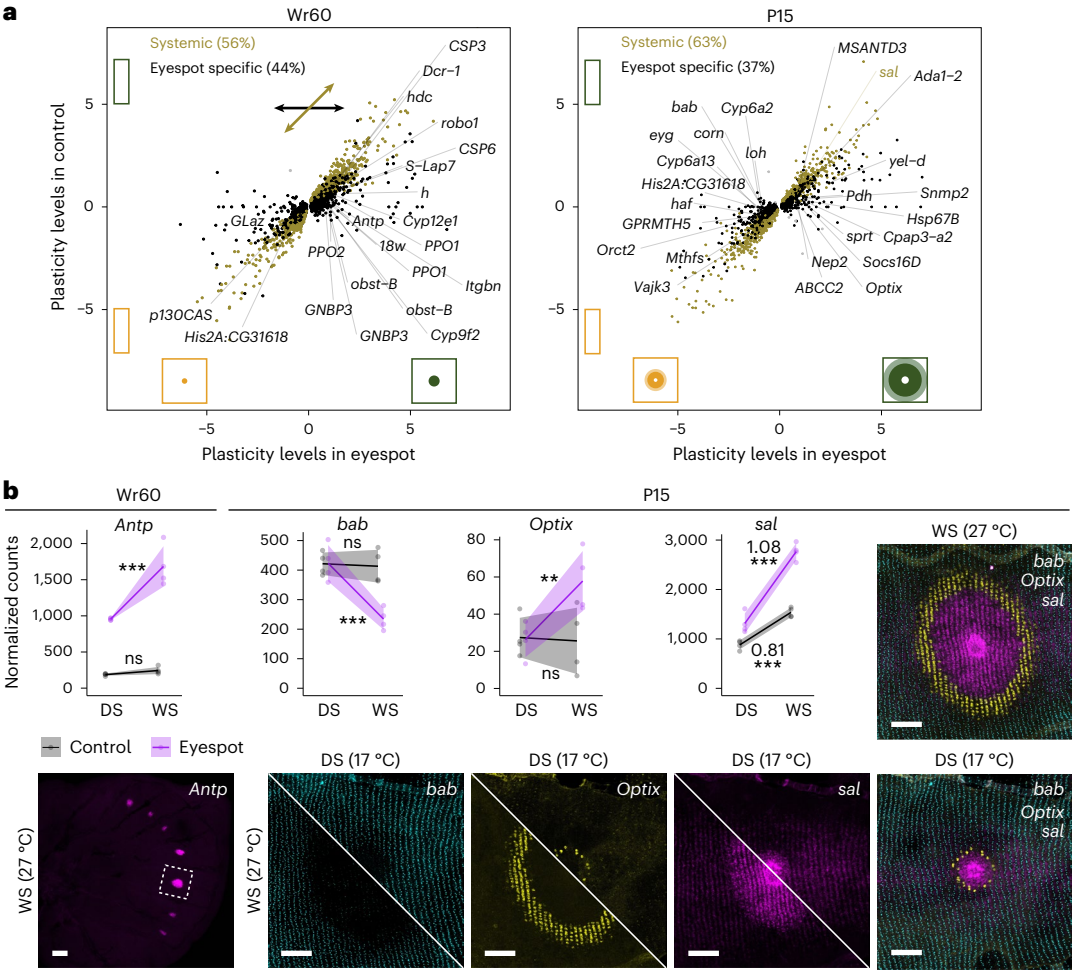

Fig. 2 | Genes showing trait-specific responses to cues are potential plasticity regulators. a, Plasticity levels (log_2 fold changes in gene expression across seasonal forms) of the plastic genes (differentially expressed across seasonal forms, padj < 0.05) in eyespots are plotted against their plasticity levels in the control tissue. Shortlisted genes with eyespot-specific plasticity are labelled (for those with known gene symbols). Candidate genes (Wr60: *Antp*, *h*, *18w*, *PPO1*; P15: *bab*, *Optix*, *sal*, *eyg*, *Hsp67B*) were picked for in vivo staining and/or functional validations. **b**, Expression patterns of several candidate genes are well supported by HCR staining, where *bab*, *Optix* and *sal* are expressed in the plastic eyespot ring patterns during P15. For *sal*, different plasticity levels (log_2 fold changes) across tissue types are highlighted. During the early Wr60 stage, *Antp* showed eyespot-specific plasticity, with high expression levels in wet-season eyespot centre cells. WS, wet season; DS, dry season. For RNA-seq, $n = 4$ replicates. Lines with error bands represent mean values ± 95% confidence interval (95CI). Differential gene expression was assessed (two-tailed) using the default Wald test, and *p* values were adjusted using the default Benjamini–Hochberg procedure in DESeq2 (padj: eyespot: 2.6×10^{-14} (*Antp*), 6.4×10^{-8} (*bab*), 0.0050 (*Optix*), 2.1×10^{-25} (*sal*); control: 0.11 (*Antp*), 0.89 (*bab*), 0.92 (*Optix*), 1.6×10^{-16} (*sal*)). ns, not significant; *padj < 0.05; **padj < 0.01; ***padj < 0.001. For HCR, $n = 3$ replicates. Scale bar: 100 microns.

forms. As a result, both exhibited eyespot-specific plasticity, with correlated size changes of the corresponding eyespot ring colour elements across seasonal forms (Fig. 2b).

We identified multiple essential regulators showing trait-specific plastic responses across eyespot development (Fig. 2b). On the basis of its confirmed role in eyespot size regulation and its early response to temperature, we decided to further investigate the role of *Antp* in regulating eyespot size plasticity using functional tools and in a comparative framework.

Antp regulates temperature-mediated satyrid eyespot size plasticity

Antp was recruited to butterfly eyespot centre cells at the base of Satyrinae[28–30], concurrently with the estimated evolutionary origin of temperature-mediated eyespot size plasticity in the same clade[17]. To investigate the role of *Antp* in regulating eyespot size plasticity, we focused on two satyrid butterflies, *B. anynana* and *Mycalesis mineus*, which both increase eyespot size with increasing temperature[16], and a non-satyrid outgroup species, *Junonia almana*, with limited decreases in eyespot size with increasing temperature[17] (Fig. 3a,f,k and Supplementary Fig. 5).

We used immunostaining to examine the expression and expression plasticity of *Antp* at the protein level, during 30–40% Wr stage in all three species. Antp protein was present in satyrid hindwing eyespot centres across both seasonal forms, but it was absent in the non-satyrid *J. almana* (Fig. 3b,g,l and Extended Data Fig. 2). The size of the Antp protein expression domain was significantly larger in wet-season relative to dry-season eyespot centres, across all seven hindwing eyespots in *B. anynana* and across five out of seven hindwing eyespots in *M. mineus* (Methods, Fig. 3c,h, Extended Data Fig. 3 and Supplementary Table 6). These results confirmed the taxon-specific eyespot expression of *Antp* in Satyrinae, validated the eyespot-specific expression plasticity of *Antp* at the protein level and suggested that this temperature-sensitive expression of *Antp* in eyespots is probably conserved across Satyrinae.

To test whether *Antp* regulates satyrid eyespot size plasticity, we knocked out *Antp* in both satyrids with CRISPR-Cas9-mediated genome editing and generated mosaic knockout (mKO) crispants—animals with random parts of the body mutated with a mix of mutations. We

https://doi.org/10.1038/s41559-025-02891-5

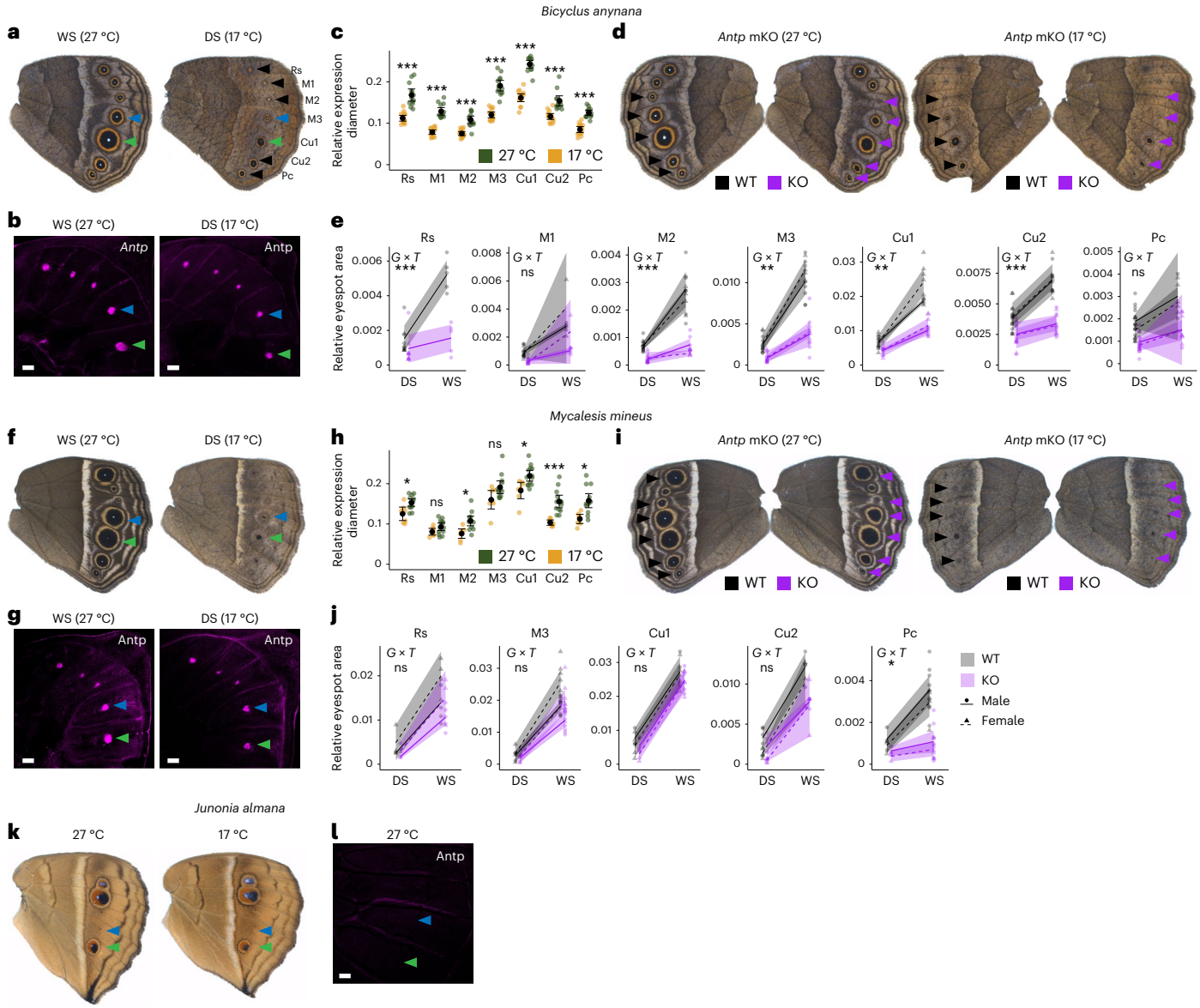

Fig. 3 | *Antp* regulates temperature-mediated eyespot size plasticity in satyrid butterflies. a–**l**, Satyrid butterflies, *B. anynana* (**a**–**e**) and *M. mineus* (**f**–**j**) show strong positive responses in hindwing eyespot size in response to temperature, but a non-satyrid *J. almana* (**k**,**l**) shows limited negative responses. WS, wet season; DS, dry season. Immunostaining shows eyespot expression of Antp protein in *B. anynana* (**b**) and *M. mineus* (**g**) across both seasonal forms during 30–40% Wr stage. Sizes of eyespot expression domains of Antp protein, represented as relative expression diameter (Methods and Extended Data Fig. 3), were compared (two-tailed) across seasonal forms in a one-way ANCOVA in *B. anynana* ($n = 14$ (DS) and 13 (WS) individuals; padj: 2.6×10^{-8} (Rs), 3.6×10^{-11} (M1), 6.4×10^{-7} (M2), 2.0×10^{-10} (M3), 9.7×10^{-11} (Cu1), 1.8×10^{-6} (Cu2), 1.5×10^{-8} (Pc)) (**c**) and *M. mineus* ($n = 7$ (DS) and 13 (WS) individuals; padj: 0.037 (Rs), 0.47 (M1), 0.037 (M2), 0.19 (M3), 0.038 (Cu1), 0.00092 (Cu2), 0.018 (Pc)) (**h**). Black dots with error bars represent mean values ± 95CI. Full statistical results are summarized in Supplementary Table 6. **l**, Eyespot expression of Antp protein is absent in *J. almana* ($n = 3$ individuals). Eyespot size was quantified across mosaic knockout (mKO) crispants in *B. anynana* (**d**) and *M. mineus* (**i**) with paired wild-type (WT) and KO eyespots, and changes in eyespot size plasticity levels were assessed (two-tailed) in a two-way ANCOVA, indicated by a significant (padj < 0.05) genotype (G) × temperature (T) interaction, in *B. anynana* ($n = 31$ (WS) and 50 (DS) mKO crispants; padj: 0.00060 (Rs), 0.12 (M1), 0.00043 (M2), 0.0035 (M3), 0.0028 (Cu1), 0.00068 (Cu2), 0.58 (Pc)) (**e**) and *M. mineus* ($n = 24$ (WS) and 16 (DS) mKO crispants; padj: 0.76 (Rs), 0.58 (M3), 0.92 (Cu1), 0.055 (Cu2), 0.030 (Pc)) (**j**). Lines with error bands represent mean values ± 95CI. Numbers of eyespots with paired phenotypes from the mKO crispants are summarized in Supplementary Table 7. Full statistical results are summarized in Supplementary Table 8. For **c**, **e**, **h** and **j**, p values were adjusted for multiple comparisons using the Benjamini–Hochberg procedure. ns, not significant; *padj < 0.05; **padj < 0.01; ***padj < 0.001. Scale bar: 100 microns.

reared these mKO crispants at 17 °C and 27 °C (Supplementary Fig. 3 and Supplementary Tables 3 and 4), leading to the development of both seasonal forms. When *Antp* was disrupted around the eyespot wing regions, hindwing eyespots became smaller without white centres in both species, but the size reduction was less noticeable in *M. mineus* (Fig. 3d,i). Other previously reported phenotypes were also observed[26] (Extended Data Figs. 4 and 5). We quantified the hindwing eyespot area from all the mKO crispants with paired eyespot phenotypes—individual butterflies with white centres mostly disappeared on one-wing (KO) and wild-type (WT) eyespots (white centres intact) on the other wing (Fig. 3d,i). We assigned these phenotype-inferred genotypes, 'WT' and 'KO', to the eyespots with corresponding phenotypes, and tested whether plasticity levels differed in WT and KO eyespots, by testing the presence/absence of a significant genotype × temperature ($G \times T$) interaction on eyespot size. We observed significant $G \times T$ interactions for five out of seven eyespots in *B. anynana* and one out of five

eyespots in *M. mineus* (only five eyespots are consistently visible in this species) (Fig. 3e,j and Supplementary Tables 7 and 8). This suggests that the recruitment of *Antp* to satyrid eyespots increased the size of hindwing eyespots in a temperature-dependent way, increasing their plasticity levels. The impact of *Antp* on the plasticity levels, however, varies across the two species examined, being stronger in *B. anynana*.

A novel promoter *P1* activates *Antp* expression in satyrid eyespots

After confirming that *Antp* plays a likely conserved role in regulating eyespot size plasticity in satyrid butterflies, we sought to investigate how *Antp* gained its eyespot-specific expression. Combining our newly generated data with a comprehensive set of published tissue-specific gene expression datasets[31,32] (Fig. 4a and Supplementary Table 9), we found that *Antp* is predominantly expressed in embryos, legs, prolegs and wing eyespots in *B. anynana* (Fig. 4b). As context-specific gene expression can be achieved via alternative promoters[33,34], we inspected the annotated gene model of *Antp* in the *B. anynana* ilBicAnyn1.1 genome[35] and found nine annotated *Antp* transcripts sharing identical coding sequences (CDS) but driven by six alternative promoters. Each promoter is associated with a unique first exon that codes for a 5′ untranslated region (5′UTR) (Fig. 4c left panel and Extended Data Fig. 6). To test whether any of these alternative promoters activate *Antp* expression specifically in eyespots, we performed promoter usage analysis, to identify the proportion of total *Antp* expression driven by each promoter in each tissue (Fig. 4c, middle panel). In this analysis, promoter activity was inferred by quantifying the RNA-seq junctions aligning to the first intron of the transcripts initiated at each promoter[34]. We noticed that the first distal promoter (*P1*) is exclusively activated in eyespots (Fig. 4c, middle panel), showing a junction in the first intron of a transcript initiated by *P1* only in eyespots (Fig. 4c, right panel). In larval eyespots, it drives over 60% of total *Antp* expression, whereas the remaining expression is entirely driven by the second distal promoter (*P2*) (Fig. 4c, middle panel). In contrast to *P1*, *P2* is activated across all tested tissues/developmental stages, rendering it a pleiotropic promoter, and it drives almost the entire *Antp* expression in non-eyespot larval wing tissues (Fig. 4c, middle and right panels).

To test the extent of sequence conservation of *Antp* promoters across Lepidoptera, we blasted each *B. anynana Antp* promoter, and each CDS, against genomes of all sequenced satyrids and eyespot-bearing butterflies with prior temperature-mediated plasticity data and/or eyespot expression data on *Antp*. For this purpose, we also assembled and included a draft genome for *J. almana*. We found that while *Antp P2-6* and the two CDSs are all deeply conserved across Lepidoptera, *P1* is exclusively present in Satyrinae, although a fragmented orthologous sequence is present in the outgroup *Junonia* (Fig. 4d). As sequence conservation does not directly indicate conservation in promoter activity[36], we inspected whole transcriptomic annotations of two non-satyrids with eyespots—*Junonia coenia*[37] and *Vanessa cardui*, for an unbiased examination of transcriptional activities around *Antp*. There are no annotated *Antp* transcript initiated from the orthologous genomic region of *P1*, even when a partial *P1* sequence is present in *J. coenia* (Extended Data Fig. 6). This suggests that an active *P1* might have evolved exclusively in Satyrinae.

To directly detect promoter activities within and outside Satyrinae, we used HCR to co-stain the promoter-specific first exons of *P1* and *P2* and *Antp CDS* in larval wings of *B. anynana*, *M. mineus* and *J. almana*, and *B. anynana* embryos (Supplementary Fig. 6). We found that *Antp* CDS, *P1* and *P2* were all highly activated in satyrid eyespots, and conversely, none could be visibly detected in *Junonia* eyespots (Fig. 4e and Extended Data Fig. 2). In *B. anynana* embryos, *Antp* CDS was present in a highly tissue/cell-specific manner across the body except the head, *P2* was activated mainly in the T2 segment and *P1* was not detected (Fig. 4e and Supplementary Fig. 7). All lines of evidence presented above strongly suggest that a novel, taxon-specific *Antp* promoter, *P1*, actively drives *Antp* expression specifically in satyrid eyespots. Also, as *P2* is highly activated in satyrid eyespots only in the presence of an active adjacent *P1* (Fig. 4e), *P1* might also serve as a novel modular enhancer that boosts the transcriptional activity of the ancestral, pleiotropic *P2* in satyrid eyespots[38].

Antp P1 regulates temperature-mediated satyrid eyespot plasticity

To examine the roles of *P1* and *P2*, we generated mKO crispants by co-injecting two guide RNAs to introduce long deletions around the conserved region (Fig. 4d, middle and right panels), essential for promoter functions[39,40], of each promoter in *B. anynana* (Fig. 5a, Extended Data Figs. 7 and 8 and Supplementary Tables 3 and 4). Whereas *P2* mKO crispants with high-penetrance long deletions did not show visible phenotypic changes (Fig. 5a, right panel; Extended Data Fig. 7 and Supplementary Table 4), 27–40% *P1* mKO crispants showed smaller hindwing eyespots without white centres (Extended Data Fig. 8 and Supplementary Table 4), suggesting that *P1*, but not *P2*, is necessary to mediate visibly detectable changes in eyespot size. To test if *P1* plays a role in regulating eyespot size plasticity levels, we crossed *P1* mKO crispants with WT and then crossed two genetically identical F1 heterozygotes, with a 252 bp deletion around *P1*, with each other. We then reared the resulting F2 offspring across two temperatures (Methods). Among F2 animals, whereas mutant heterozygotes ($P1^{+}/P1^{\Delta 252}$) were visibly indistinguishable from WT ($P1^{+}/P1^{+}$) animals, mutant homozygotes ($P1^{\Delta 252}/P1^{\Delta 252}$) showed smaller hindwing eyespots without white centres (Fig. 5a and Extended Data Fig. 9). We compared hindwing eyespot size plasticity levels across sib-paired $P1^{+}/P1^{+}$, $P1^{+}/P1^{\Delta 252}$ and $P1^{\Delta 252}/P1^{\Delta 252}$ animals and found that whereas $P1^{+}/P1^{\Delta 252}$ heterozygotes exhibited indistinguishable plasticity levels compared with $P1^{+}/P1^{+}$ WT siblings, $P1^{\Delta 252}/P1^{\Delta 252}$ mutants exhibited significantly reduced plasticity levels across four out of seven hindwing eyespots compared with $P1^{+}/P1^{+}$ WT siblings (Fig. 5b, Extended Data Fig. 10 and Supplementary Tables 10 and 11). This indicates that the taxon-specific *Antp P1* promoter increases temperature-mediated satyrid eyespot size plasticity in *B. anynana*.

Discussion

In this study, we generated a tissue-specific transcriptome to resolve trait-specific development of butterfly eyespot size plasticity. We found multiple essential regulators showing trait-specific responses to temperature across the eyespot gene-regulatory network (GRN). On the basis of these discoveries, we propose a possible developmental model of this classic case of adaptive phenotypic plasticity (Fig. 6a). Temperature inputs are predominantly sensed and integrated into the eyespot GRN during the larval–pupal transition, partially via altered dynamics of 20E and/or other mechanisms. This sensation and integration of cues could potentially happen at multiple time points within the sensitive period and even before the surge of larval 20E titres, when *Antp* is already showing asymmetrical expression domains in eyespot centre cells across seasonal forms (Fig. 3). During the pupal eyespot centre signalling stage, the integrated plastic responses from the upstream regulators lead to different levels of signalling molecules, potentially morphogens *wingless* (*wg*) and/or *decapentaplegic* (*dpp*) from the centre[41,42] that subsequently orchestrate master colour regulators (*bab*, *Optix*, *sal*, *Antp*) in the surrounding cells to pre-pattern the final eyespot rings with different sizes across seasonal forms (Fig. 6a). Future studies are expected to elucidate the underlying GRN in the development of plasticity.

We identified a taxon-specific promoter that activates *Antp* expression in butterfly eyespot wing patterns in a temperature-sensitive manner. This promoter, estimated to have evolved ~60 million years ago at the base of Satyrinae, concurrently with the estimated evolutionary origin of *Antp* recruitment in butterfly eyespots[28–30], might have facilitated the concurrent evolution of temperature-mediated eyespot size plasticity in this clade, under the phylogenetic resolution we have

https://doi.org/10.1038/s41559-025-02891-5

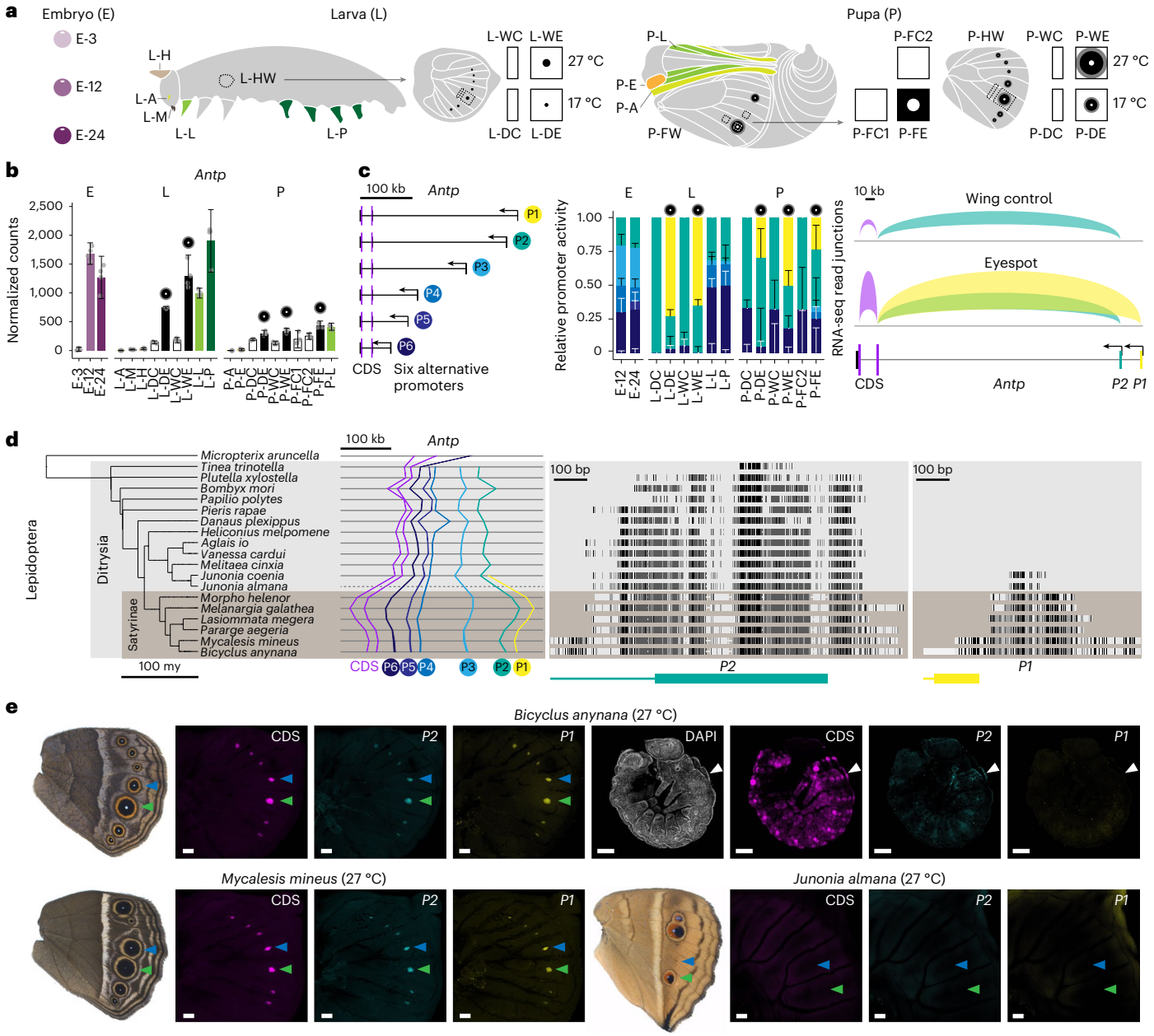

Fig. 4 | A novel promoter activates *Antp* expression in satyrid eyespots. **a**, A comprehensive tissue-specific transcriptomic dataset used in the *Antp* gene expression and promoter usage analysis. Tissue codes follow the form of 'stage–tissue type'. Stages: E, embryo, number indicates hour post-oviposition; L, larva; P, pupa. Tissue types: H, head horn; A, antenna; M, maxilla; L, T1 leg; P, proleg; E, eye; FW, forewing; HW, hindwing; WC, wet-season hindwing non-eyespot control; WE, wet-season hindwing eyespot; DC, dry-season hindwing non-eyespot control; DE, dry-season hindwing eyespot; FE, forewing eyespot; FC1 and 2, forewing non-eyespot control. Data sources and a full description of tissue codes are summarized in Supplementary Table 9. **b**, *Antp* expression across tissue types and development. **c**, Left panel: gene model of *B. anynana Antp* reveals six alternative promoters, each associated with a unique first exon, coding for a 5′ untranslated region; middle panel: relative promoter activity—the proportion of RNA-seq junction reads aligning to the first intron of the transcripts initiated at each promoter; right panel: RNA-seq junctions in the first introns showing different promoter usage across larval eyespot and non-eyespot control wing tissues. For RNA-seq, $n = 4$ replicates. For **b** and **c** middle panels, data are represented as mean values ± 95CI. **d**, Left panel: local synteny mapping of all *Antp* promoters and CDSs across Lepidoptera. The highly fragmented *J. almana* genome assembly is not visualized (dotted line). Middle and right panels: sequence conservation of *P1* and *P2*, the two promoters activated in larval wings. Aligning promoter regions were indicated by black–grey vertical lines, with darker lines showing higher sequence conservation. Coloured bars (cyan and yellow) denote annotated *Antp* transcripts initiated at each promoter, where the first exons are thickened. Phylogeny is from refs. 20,61,62. **e**, HCR co-staining of *Antp CDS* and the first exons associated with *P1* and *P2*, across *B. anynana*, *M. mineus*, *J. almana* larval wings and *B. anynana* 48 h embryos. For HCR, $n = 3$ replicates. Scale bar: 100 microns.

reached so far[17] (Fig. 6b). Due to the polygenic nature of plasticity on a microevolutionary scale[7,9,10], we believe that *Antp* is not the sole or ultimate plasticity regulator across all extant satyrids. This is evidenced by a residual plasticity in *Bicyclus* when *Antp* was disrupted and its less predominant role in *Mycalesis* (Fig. 3e,j). Instead, we propose that *Antp*-mediated plasticity potentially emerged early in satyrids, evolved in amplitude and was modified as a result of developmental systems drift, leading to lineage-specific mechanisms across extant satyrids. In *Bicyclus*, this ancestral mechanism still plays a predominant role, whereas lineages such as *Mycalesis* evolved other predominant

https://doi.org/10.1038/s41559-025-02891-5

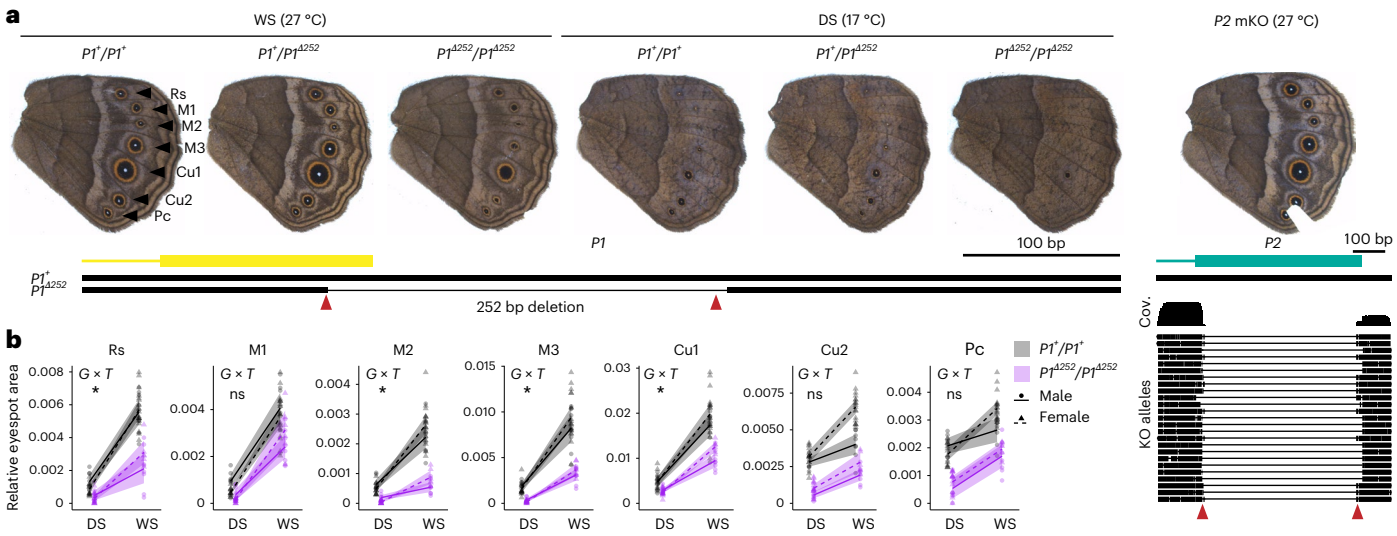

Fig. 5 | *Antp P1* regulates satyrid eyespot size plasticity. a, Conserved promoter regions (as shown in Fig. 4d) around *Antp P1* and *P2* were disrupted in *B. anynana* using CRISPR-Cas9. Coloured bars (yellow and cyan) denote annotated *Antp* transcripts initiated at each promoter, where the first exons are thickened. Whereas mosaic knockout (mKO) crispants were generated for *P2*, a mutant line carrying a 252 bp deletion was generated for *P1*. Red arrowheads denote guide RNA cut sites. *P2* mKO crispants were genotyped via Nanopore amplicon sequencing. Sequence coverage (Cov.) across the amplicon and major KO alleles are shown. WS, wet season; DS, dry season. **b**, Changes in eyespot size plasticity levels were assessed (two-tailed) across sib-paired WT ($P1^{+}/P1^{+}$, $n = 27$ (WS) and 20 (DS) individuals) and mutant homozygotes ($P1^{\Delta 252}/P1^{\Delta 252}$, $n = 14$ (WS) and 22 (DS) individuals) and across sib-paired WT ($P1^{+}/P1^{+}$) and mutant heterozygotes ($P1^{+}/P1^{\Delta 252}$, $n = 30$ (WS) and 33 (DS) individuals; Extended Data Fig. 10), in a two-way ANCOVA, indicated by a significant (padj < 0.05) genotype (*G*) × temperature (*T*) interaction (padj: 0.021 (Rs), 0.81 (M1), 0.014 (M2), 0.046 (M3), 0.016 (Cu1), 0.72 (Cu2), 0.16 (Pc)). Lines with error bands represent mean values ± 95CI. Detailed sample sizes are summarized in Supplementary Table 10. Full statistical results are summarized in Supplementary Table 11. *P* values were adjusted for multiple comparisons using the Benjamini–Hochberg procedure. ns, not significant; *padj < 0.05; **padj < 0.01; ***padj < 0.001.

mechanisms and lineages such as the neotropical *Morpho* lost most plasticity despite retaining *Antp* expression in eyespots[17,30] (Fig. 6b). Whereas early diversification of Satyrinae was proposed to be driven by the simultaneous radiation of their grass host plants, triggered by dramatic prehistorical climate changes[43], we hypothesize that the evolution of eyespot size plasticity, via this novel promoter, could be an alternative/complementary driver. Future work on more densely sampled satyrid species, with a known biogeographical history, will further resolve how a complex system of adaptive plasticity evolved, helping to guide future conservation efforts in an era of intensifying climate change[44].

Whereas recent advances illustrate how nuanced modifications in ancestral cis-regulatory elements create phenotypic novelties[32,45–49], including the adaptive circadian plasticity in *Drosophila* flies[50], our study emphasizes the importance of novel cis-regulatory elements in fuelling adaptive phenotypic evolution. Novel cis-regulatory elements might have a higher potential to both (1) drive gene expression in novel developmental contexts[51] and (2) bypass the pleiotropy of ancestral regulatory elements[52,53], aiding the emergence of phenotypic novelties. In this case, a novel promoter emerged in a Hox gene previously associated with butterfly eyespots[28–30], fuelled the evolution of adaptive environmental sensitivity in that trait.

Methods

Insect husbandry

Lab populations of *B. anynana* butterflies have been reared in the laboratory since 1988, originally collected in Malawi. *M. mineus* butterflies were collected from Clementi Forest, Singapore, *J. almana* butterflies were collected from Seletar West Farmway, Singapore, both under a National Parks Board permit (NP/RP14-063-7a).

All the butterflies were reared in two climate rooms, at 17 °C and 27 °C, leading to the development of dry-season form and wet-season form, respectively. Both climate rooms have a 12:12 day: night cycle (daytime and nighttime start from 7 a.m. and 7 p.m., respectively), with 60% relative humidity. *B. anynana* and *M. mineus* larvae were fed young corn leaves, and adults were fed mashed banana. *J. almana* larvae were fed *Ruellia repens*, and adults were fed artificial nectar.

Temperature-shift experiments

Temperature-shift schemes included individual or combinations of six non-overlapping short developmental windows spanning the entire fifth instar larval stage and the first 15% pupal stage in *B. anynana* (Extended Data Fig. 1, left panel). Females were reared at 27 °C, shifted to 17 °C for the designated developmental windows or combinations of windows, followed by a shift back to 27 °C.

For the schemes involving wanderer, pre-pupal and pupal stages, the start and end time points of these stages were precisely scored for each individual using the time-lapse function of an Olympus Tough TG-5 camera[4]. One exception was shifting the entire fifth instar larval stage (L5). The pupation time points of this scheme were largely dispersed among individuals due to the long rearing durations (~20 days) at 17 °C. For this scheme, individual pupation status was checked manually every 6 h throughout the day, and fresh pupae were shifted back to 27 °C in a timely basis.

For the schemes involving pre-wanderer fifth instar larval stages (L5-1, -2, and -3), fourth larval ecdysis could happen throughout the day, so fourth instar larvae were checked every 6 h throughout the day. If they entered fifth instar larval stage between 12 a.m. and 12 p.m. of a day, that day was considered day 0 of the fifth instar larval stage; if they entered fifth instar larval stage between 12 p.m. and 12 a.m., the next day was considered day 0. The shift start time of these schemes was 12 a.m. at midnight, and shift durations lasted 5 days. Because the developmental pace of the pre-wanderer stages could vary by 1–2 days among individuals, animals with the actual shift schemes overlapping more than 50% of the adjacent shift schemes were excluded as they did not represent a genuine effect of the designated shift schemes anymore.

The temperature-shift experiments were performed by grouping 3–8 females perfectly synchronized in development in small plastic

https://doi.org/10.1038/s41559-025-02891-5

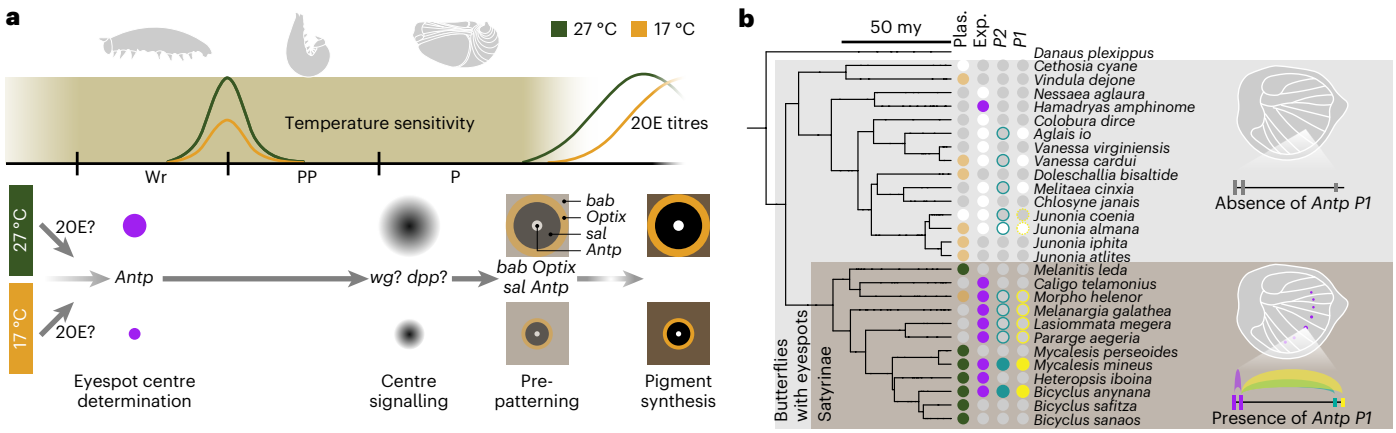

Fig. 6 | An evolutionary–developmental model of a classic system of adaptive phenotypic plasticity. a,**b**, We propose a developmental model of temperature-mediated eyespot size plasticity, where *Antp* sits upstream of the eyespot gene-regulatory network (GRN) (**a**), and an evolutionary model illustrating how plasticity evolved on a phylogeny (**b**). The phylogeny summarizes all the current knowledge about temperature-mediated eyespot plasticity (Plas.), eyespot expression of Antp protein (Exp.) and sequence/activity conservation of *Antp* promoters *P1* and *P2*. Plas.: green: strong positive eyespot size response to temperature; orange: limited negative response to temperature; white: no significant response. Exp.: magenta: Antp protein expression in eyespots; white: no Antp eyespot expression. *P1* and *P2*: coloured outline: sequence conservation (dotted outline denotes limited conservation); fill colour: coloured: presence of promoter activities; white: absence of promoter activities/sequence conservation. Grey: unknown. Phylogeny is from refs. 20,61.

containers. Each shift scheme included at least 20 females, except for L5-3, where 12 females were used. Statistics of the temperature-shift experiments were summarized in Supplementary Table 1.

Adult butterflies were frozen around 4 h after adult eclosion. Wings were dissected and imaged with a Leica DMS 1000 microscope, using 1.25× magnification level and a Leica 0.32× Achromat objective lens. Ventral hindwing Cu1 eyespot areas and whole hindwing areas were measured in pixels using the Quick Selection Tool in Photoshop 2021.

Calculation of temperature sensitivity in eyespot size

As different temperature-shift schemes involved different shift durations, we define temperature sensitivity in eyespot size as reductions in relative eyespot size, compared with unshifted (wet-season) eyespots, per unit shift time (h). Under this definition, relative eyespot size (eyespot area divided by hindwing area) was calculated for Cu1 eyespots across the six non-overlapping shift schemes (L5-1, -2, -3, Wr, PP, P15) and in the wet-season form. Temperature sensitivities in eyespot size were then calculated as:

$$\text{Temperature sensitivity} = (\text{Mean relative eyespot size of wet-season form} - \text{relative eyespot size of the shift scheme})/\text{Mean shift duration}$$

Temperature sensitivity values were then compared across the six non-overlapping shift schemes in a statistical test.

Laser microdissection and RNA sequencing

Seasonal forms of *B. anynana* were precisely staged as previously described[4]. Female hindwings were dissected from wet-season and dry-season forms at 60% wanderer (Wr60) and 15% pupal (P15) stages. Laser microdissection was performed according to a published protocol[54]. In brief, freshly dissected wings were immediately mounted on polyethylene naphthalate (PEN) membrane slides on ice, then fixed and dehydrated using ice-cold ethanol and acetone and stained using ThermoFisher Arcturus HistoGene Staining Solution. Fixed and dehydrated tissue slides were kept at −80 °C until enough samples were collected. Laser microdissection was performed to cut the eyespot tissue and an adjacent non-eyespot control tissue from the hindwing sector Cu1. For the Wr60 stage, we cut a rectangular area within the Cu1 sector for the eyespot tissue, centred on Cu1 eyespot centre. For the P15 stage, we cut an inscribed circular area within Cu1 sector to sample the entire eyespot pattern, centred on the Cu1 eyespot centre. In both developmental stages, we cut a narrow rectangular area just next to the proximal side of the Cu1 eyespot region within the Cu1 sector as a control wing tissue. One biological replicate included microsections pooled from 30 hindwings from 15 individuals (both sides) for the Wr60 stage or eight hindwings from eight individuals (one side only) for the P15 stage. Four biological replicates were included for each condition. For a brief tissue digestion before RNA extraction, microsections were collected and pooled in lysis buffer and digested using proteinase K at 55 °C for 9 min. Total RNAs were extracted using mirVana miRNA Isolation Kit following the manufacturer's instructions.

Quality check for total RNA samples was performed using Nanodrop 2000, gel electrophoresis and LabChip. Poly-A enriched stranded mRNA sequencing libraries were constructed using VAHTS Universal V8 RNA-seq Library Prep Kit. For Illumina sequencing, over 30 million 150 bp read pairs per sample were generated using Illumina NovaSeq platform. Quality check, library construction and sequencing were carried out by Azenta.

Gene expression and functional enrichment analysis

Trimmomatic 0.39 was used to trim adaptors from raw sequencing reads (options: PE ILLUMINACLIP:TruSeq3-PE-2.fa:2:30:10:8:true MAXINFO:40:0.2 MINLEN:32). Adaptor-trimmed clean reads were used to quantify gene expressions (National Center for Biotechnology Information (NCBI) *B. anynana* v1.2 genome) using Salmon 1.6.0, with the quasi-mapping mode (options: –validateMappings –seqBias –gcBias). Gene expression levels were normalized, and differential gene expression analysis was performed using DESeq2 1.38.3 in R studio. Numbers and lists of differentially expressed genes (padj < 0.05) in pairwise comparisons were summarized in Supplementary Table 2 and deposited in figshare[55].

Gene set enrichment analysis was performed using Babelomics 5 for the entire list of plastic genes (differentially expressed across seasonal forms, padj < 0.05) in eyespots, and for the two subsets of the list showing systematic and eyespot-specific gene expression plasticity, at each developmental stage. Lists of enriched gene ontology terms (padj < 0.1) were deposited in figshare[55].

Promoter usage analysis

Promoter usage analysis was performed across the newly generated data and a comprehensive set of published tissue/body part-specific transcriptomic data[31,32] (Supplementary Table 9). Four biological

replicates were included in each condition. Adaptors were trimmed from raw sequencing reads as described above. Adaptor-trimmed clean reads were used to quantify gene expressions (ilBicAnyn1.1 genome[35]) using Salmon 1.6.0, with the quasi-mapping mode (options: –validateMappings –seqBias –gcBias). Gene expression levels were normalized using DESeq2 1.38.3 and the expression levels of *Antp* were checked across all samples.

To quantify splice junctions for the estimation of promoter activities, adaptor-trimmed clean reads were mapped to the ilBicAnyn1.1 genome using Spliced Transcripts Alignment to a Reference (STAR) 2.7.10a. A two-pass approach was adopted to index the genome for a more sensitive junction discovery, as described in the STAR manual. In brief, the ilBicAnyn1.1 genome was first indexed with the genome annotations for the first mapping pass across all the samples with usual STAR parameters (options: –outSJfilterReads Unique). The splice junctions detected from the first pass were merged and filtered. All the non-canonical junctions, and junctions supported by too few reads (reads ≤ 2) were discarded. The consolidated and filtered junctions were used as annotated junctions to index the genome again with the genome annotation, and the new genome index was used for a second mapping pass (options: –outSJfilterReads Unique –outFilterMultimapNmax 1). Junction files generated from the second mapping pass were used as inputs for promoter usage analysis using proActiv 1.3.4[34] in R studio. Relative promoter activities—the proportion of total *Antp* transcription initiated by each promoter, were quantified across all samples with sufficient *Antp* expression levels and junction reads to support the analysis.

J. almana genome sequencing and assembly

Genomic DNA was extracted from thorax of a female *J. almana* adult using Omega E.Z.N.A Tissue DNA Kit. Library preparation and sequencing for Illumina short-read paired-end (2 × 150 bp) sequencing were performed by Genewiz, resulting in 20 GB of raw data.

Raw FASTQ files were trimmed and quality controlled using the bbduk script from BBMap 38.96 tools. Short-read-based genome assembly was performed using Platanus 1.2.4 with default settings. The genome was first assembled into contigs using the platanus assemble command, followed by scaffolding of the assembled contigs. Finally, gaps were closed using the platanus gap_close command, resulting in a final assembly size of 476 MB.

In situ HCR

Detection of candidate genes and promoters was carried out based on the protocol described[56] with few modifications. For protein-coding genes, probes were designed on the coding sequences (CDS). For *Antp* promoters, probes were designed on an extended genomic region around the unique first exon initiated by each promoter (Supplementary Fig. 6). All the HCR probe sets were purchased from Integrated DNA Technologies (IDT). Probe sequences were deposited in figshare[55]. Wings or embryos were dissected in 1× phosphate-buffered saline (PBS) and transferred to glass chambers where they were fixed in 1× phosphate-buffered saline with tween-20 (PBST) supplemented with 4% formaldehyde for 30 min. After fixation, the tissues were treated with a detergent solution[57] and washed first with 1× PBST followed by washes in 5× saline-sodium citrate with tween-20 (SSCT). Afterward, embryos were embedded in polyacrylamide gel[58] and transferred to a confocal dish, while wings were transferred to glass wells with 500 µl of 30% probe hybridization buffer. The hybridization reaction involved incubation in a solution containing 50 µl (50 µM) of probe set against each gene in 2,000 µl of 30% probe hybridization buffer followed by rigorous washing with 30% probe wash buffer. Afterward, tissues were washed with 5× SSCT and incubated in amplification buffer for 30 min. For the chain reaction, a solution with HCR hairpins (Molecular instruments) in amplification buffer was added to the tissues followed by washes in 5× SSCT. Finally, the tissues were mounted on an in-house mounting media and imaged under an Olympus fv3000 confocal microscope. The primary incubation was carried out for 16–24 h at 32 °C and the secondary hairpin incubation for 8 h at room temperature.

Immunostaining

B. anynana and *M. mineus* female hindwings were dissected at ~30–40% wanderer stage from both seasonal forms, *J. almana* female hindwings were dissected at the same stage, from wet-season form only. Fresh wings were fixed with 4% formaldehyde in cold fix buffer (0.1 M PIPES pH 6.9, 1 mM EGTA pH 6.9, 1% Triton x-100, 2 mM $MgSO_4$) for 30 min. Fixed wings were washed four times with cold PBS and incubated in block buffer (50 mM Tris pH 6.8, 150 mM NaCl, 0.5% IGEPAL, 5 mg ml^{-1} bovine serum albumin (BSA)) overnight at 4 °C. Wings were then incubated with primary antibody diluted in wash buffer (50 mM Tris pH 6.8, 150 mM NaCl, 0.5% IGEPAL, 1 mg ml^{-1} BSA) for 24 h at 4 °C. A mouse anti-Antp 4C3 antibody (Developmental Studies Hybridoma Bank, final dilution 1:200) was used as the primary antibody. For *J. almana*, an additional guinea pig anti-Sal GP66.1 antibody[30] (final dilution 1:20,000) was used as a positive control. Wings were washed four times for 20 min each with cold wash buffer and then incubated with secondary antibody diluted in wash buffer for 2 h at 4 °C in a dark environment. For *B. anynana* and *M. mineus*, Alexa Fluor 555 Goat anti-Mouse (A-21422) was used as the secondary antibody (final dilution 1:500). For *J. almana*, Alexa Fluor 488 Goat anti-Mouse (A32723) and Alexa Fluor 555 Goat anti-Guinea Pig (A-21435, final dilution 1:500) were used for a double staining of *Antp* and *Sal*. Wings were washed four times for 20 min each with cold wash buffer, mounted on glass slides and kept at 4 °C before imaging. Ventral surfaces of the wings were imaged using an Olympus FV3000 confocal laser scanning microscope with identical configurations.

Calculation of eyespot expression diameter of Antp protein

For each hindwing eyespot of *B. anynana* and *M. mineus*, two orthogonal diameters of the Antp protein expression domain were measured, one in parallel with the proximal-distal axis of the sector, and the other perpendicular to it (Extended Data Fig. 3). The size of the Antp protein expression domain, defined as eyespot expression diameter, was calculated as the mean of the two measured diameters. The distance between the Cu1 and M3 eyespot centres was also measured and used as a hindwing size proxy, which was entered in the statistical analysis as a covariate. All diameters and distances were measured in pixels using the ruler tool in Photoshop 2021. To avoid bias, all images were measured 'blindly', without knowledge of the treatment group they belonged to.

CRISPR-Cas9 genome editing

Embryonic CRISPR-Cas9 knockout (KO) experiments were performed in *B. anynana* and *M. mineus* following the established protocol[59]. Guide RNAs were designed using CRISPRdirect. Specificity of the guide RNA target sequences was checked by blasting against the NCBI *B. anynana* v1.2 genome or the published *M. mineus* genome[60]. For protein-coding genes, template single guide DNAs (sgDNAs) were produced by PCR, using NEB Q5 High-Fidelity DNA Polymerase. sgDNAs were transcribed into sgRNAs using NEB T7 RNA Polymerase. sgRNAs were purified by ethanol precipitation. Size and integrity of sgDNAs and sgRNAs were checked using gel electrophoresis. For *Antp* promoters, synthetic crRNAs were directly ordered from IDT. Target sequences of all guide RNAs were listed in Supplementary Table 3.

For microinjection of guide RNAs, corn leaves were placed in *B. anynana* or *M. mineus* adult cages around 2–3 p.m. Leaves were left in the cages for 1 h and eggs were collected and placed onto 1-mm-wide double-sided tapes in petri dishes. For protein-coding genes, we used a final concentration of 500 ng $µl^{-1}$ IDT Alt-R S.p. Cas9 Nuclease V3 (with 1× Cas9 buffer) and 250 ng $µl^{-1}$ sgRNA in the injection mixture. The injection mixture was incubated at 37 °C for 10 min before injection. A 0.5-µl amount of food dye was added per 10 µl mixture to facilitate

the visualization of the injected solutions. Different sgRNAs for the same protein-coding gene were not mixed but injected independently. For *Antp* promoters, eggs were injected with CRISPR/Cas9 protein-crRNA-tracrRNA complexes. Stock solutions of crRNAs and tracrRNA were prepared as 1,000 ng µl, 4 µl of crRNA were incubated with 4 µl of tracrRNA and 12 µl of Nuclease-Free Duplex Buffer at 95 °C for 5 min and then left to cool down at room temperature. We used a final concentration of 500 ng μl^{-1} Cas9 protein (with 1× Cas9 buffer) and ~ 200 ng μl^{-1} annealed crRNA-tracrRNA in the injection mixture. Two crRNAs designed for each promoter were co-injected to introduce long deletions around the promoter regions.

Microinjection was performed using glass capillary needles. After injection, moistened cotton balls were placed into each Petri dish. Hatchlings were shifted to corn plants to complete development. Adults were frozen ~6 h after adult emergence. Phenotypic changes were inspected manually, and mutants were imaged using a Leica DMS 1000 microscope. The CRISPR injection statistics were summarized in Supplementary Table 4.

Quantification of eyespot size from mosaic *Antp* mutants with paired phenotypes

CRISPR-Cas9 mediated *Antp* KO experiments were performed in *B. anynana* and *M. mineus*. Injected eggs were reared at either 27 °C or 17 °C. Adult butterflies were collected and manually screened for all visible phenotypes. To examine the effect of *Antp* KO on the eyespot size plasticity levels, all crispants with paired WT and KO hindwing eyespot phenotypes—individual butterflies with *Antp* KO eyespot phenotypes on one wing and WT phenotypes on the other were used. Wings were imaged as described above. To get precise measurements of all eyespots, especially for the smaller and dry-season eyespots, wings were imaged with the same configurations, with a 4× magnification level for zoom-in views of eyespots, and a 1.25× level for whole hindwings. Eyespot areas of each ventral hindwing eyespot with paired WT and KO phenotypes, and whole hindwing areas were measured in pixels in Photoshop 2021, as described above. Eyespot size was measured across all seven hindwing eyespots in *B. anynana* and five out of seven hindwing eyespots in *M. mineus*, as *M. mineus* M1 and M2 eyespots and/or their associated white eyespot centres were not consistently observed even among WT animals. The number of eyespots with paired phenotypes was summarized in Supplementary Table 7.

T7 endonuclease assay

T7 endonuclease assays were performed to confirm the in vivo cutting efficiencies of all sgRNAs before large-scale egg injections. Genomic DNA was extracted from ~20 injected eggs, 4 days after injection, using the E.Z.N.A Tissue DNA Kit. For each target gene, one pair of genotyping (GT) primers was designed to amplify a 300–600 bp genomic region spanning the cut sites using PCRBIO Taq Mix Red. PCR products were purified using ThermoFisher GeneJET PCR Purification Kit. Two hundred ng of PCR products were denatured and re-hybridized with NEB Buffer 2 in a total volume of 20 µl, following the reported temperature settings[59]. The product was divided into two tubes, one treated with 1-µl T7 endonuclease (New England Biolabs) and the other without endonuclease as a control. Both were incubated at 37 °C for 15 min and were subsequently run on a 2% agarose gel. All guide RNAs showed efficient cutting of the designated target sites in vivo, except one *Hsp67B* guide in *B. anynana* (Supplementary Fig. 3). GT primers were listed in Supplementary Table 3.

Detect long deletions by PCR

For *Antp P1* and *P2*, efficient in vivo genomic editing by the co-injected crRNAs and the resulting long deletions were confirmed by PCR before large-scale egg injections. Genomic DNA was extracted from injected eggs using E.Z.N.A Tissue DNA Kit. GT primers (Supplementary Table 3) were designed to amplify a ~400–700 bp genomic region flanking both crRNAs for each promoter using PCRBIO Taq Mix Red. PCR products were checked using gel electrophoresis for the presence of long deletion alleles (Extended Data Figs. 7 and 8).

Genotyping *eyg* and *h* mosaic mutants via Sanger sequencing

On-target mutations across mosaic knockout (mKO) mutants of *eyg* and *h* were checked using Sanger sequencing. Genomic DNA was extracted from a single wing showing mutant phenotypes from each mKO mutant using E.Z.N.A Tissue DNA Kit. The same GT primers used in the T7 assay were used to amplify the genomic region spanning the target sites using PCRBIO Taq Mix Red. PCR products were purified using ThermoFisher GeneJET PCR Purification Kit and were sent for Sanger sequencing by 1st Base (Axil Scientific Pte Ltd.). Guide-induced indels were checked using the Synthego ICE Analysis tool v3. Genotyped individuals and their indel rates were shown in Supplementary Table 5.

Genotyping *Antp P2* mosaic mutants via Nanopore sequencing

Because *Antp P2* mKO mutants did not exhibit any visible phenotypic changes, on-target long deletions were first checked with PCR. Genomic DNA was extracted from right hindwings of eight mKO females using E.Z.N.A Tissue DNA Kit. GT primers used for genotyping injected eggs were used to amplify the genomic region flanking the two crRNAs using NEB Q5 High-Fidelity DNA Polymerase, and PCR products were purified using ThermoFisher GeneJET PCR Purification Kit. PCR products were checked using gel electrophoresis and NanoDrop, and three samples showing clear long deletions (Extended Data Fig. 7) were sent for Nanopore amplicon sequencing to generate 1-GB data for each sample. Quality check, library preparation and sequencing were carried out by Azenta. Nanopore long reads were mapped to the reference sequence of *Antp P2* from the ilBicAnyn1.1 genome using minimap2 2.26, and alignments were visualized in Integrated Genomics Viewer (IGV) 2.17.3 (Fig. 5 and Extended Data Fig. 7).

Generation of *Antp P1* mutant line and eyespot quantification

Both crRNAs targeting *Antp P1* were co-injected to generate F0 *P1* mKO mutants. F0 mKO females showing eyespot phenotypes were crossed with WT males. Some of these F0 females might carry one or several mutant alleles in the germline and passed the mutant alleles to F1. The F1 offspring were screened via haemolymph extraction and Sanger genotyping, as described below.

To screen F1, around 10 µl of haemolymph was extracted from the fifth instar larvae and suspended in 200-µl Saline-Sodium Citrate buffer. Hemocytes were collected by centrifugation, then resuspended and incubated in 20-µl digestion buffer (1.1-ml 1 M Tris-HCl of pH 6.8 in 50-ml deionized water) with 2-µl proteinase K (New England Biolabs) at 37 °C for 15 min. Upon heat inactivation of proteinase K at 95 °C for 3 min, 3 µl of the cell lysate containing genomic DNA was used for PCR using designed GT primers (Supplementary Table 3). PCR products were run on the gel, F1 heterozygotes carrying long deletions showed two bands, the upper WT bands and the lower mutant bands. To isolate different long deletion alleles, the mutant bands were excised from the gel, purified using ThermoFisher GeneJET Gel Extraction Kit and sent for Sanger Sequencing by 1st Base (Axil Scientific Pte Ltd.). Among all mutant alleles, we obtained at least two F1 heterozygotes of the opposite sex carrying a frequently occurring 252 bp deletion.

The two F1 heterozygotes were crossed with each other, and the resulting F2 eggs were equally split and reared at either 27 °C or 17 °C, generating sib-paired mutant homozygotes, heterozygotes and WT in both seasonal forms. F2 adults were frozen ~6 h after adult emergence for (1) genotyping and (2) eyespot quantification. Heads were used for DNA extraction, PCR and gel electrophoresis for genotyping purposes, as described above. A sample gel image showing bands of mutant homozygotes, heterozygotes and WT is shown in Extended Data Fig. 9.

Hindwings were imaged as described above, with a 4× magnification level for zoom-in views of eyespots and a 1.25× level for whole

hindwings. Eyespot areas of each ventral hindwing eyespot, and whole hindwing areas, were measured in pixels in Photoshop 2021, as described above. Eyespots were measured 'blindly', without knowledge of the genotype they belonged to. The number of eyespots from F2 animals analysed, and their genotypes were summarized in Supplementary Table 10.

Sequence conservation of the *Antp* features

Sequence conservation of *Antp CDSs* and promoters (*P1-6*) were checked across Lepidoptera, including all sequenced satyrids and other eyespot-bearing butterflies with published data on temperature-mediated eyespot size plasticity[17,18] and/or eyespot expression of *Antp*[28–30]. *B. anynana* ilBicAnyn1.1 genomic sequences of *Antp* features were blasted against the selected lepidopteran genomes to check for the presence of any orthologous sequences in each genome.

Statistical analysis

A one-way analysis of covariance (ANCOVA) was used to test (two-tailed) the impact of temperature-shift schemes on (1) the size of the ventral hindwing Cu1 eyespot (2) the temperature sensitivity of the ventral hindwing Cu1 eyespot size and (3) the impact of rearing temperatures on the eyespot expression diameter of Antp protein in each ventral hindwing eyespot. In the case of (1) and (3), hindwing area and hindwing size proxy, respectively, was used as a covariate. Homogeneity of variances was first tested using Levene's test. On the basis of the test results, data were square root transformed to reduce skewness, when necessary. A one-way ANCOVA was performed in R studio with type III sums of squares. For (1) and (2), Tukey's multiple comparison test was used to detect which shift schemes produced significant ($p < 0.05$) changes in eyespot size or temperature sensitivity. For (3), p values were corrected for multiple comparisons using the Benjamini–Hochberg procedure.

A two-way ANCOVA was used to test (two-tailed) the impact of genotype (G), temperature (T) and their interactions ($G \times T$) on the eyespot size from (1) *Antp* mKO crispants and (2) sib-paired *Antp P1* KO lines, controlled for hindwing area and sex as covariates. Homogeneity of variances was first tested using Levene's test, and the data were square root transformed, when necessary. A two-way ANCOVA was performed in R studio with type III sums of squares, using the model: Eyespot_area ~ Wing_area + Sex + Temperature × Genotype. P values were corrected for multiple comparisons using the Benjamini–Hochberg procedure.

For the analysis mentioned above, figures were made using means and 95% CIs of the ratio of eyespot area (or eyespot expression diameter) / wing area (or wing size proxy) to visualize the distribution of the original datapoints.

Reporting summary

Further information on research design is available in the Nature Portfolio Reporting Summary linked to this article.

Data availability

All data required for reproducing and extending the study are available in the main text or the Supplementary Information. Raw RNA-seq data for *Bicyclus anynana* are available under NCBI BioProject PRJNA1268022. Raw genome sequencing and assembly data for *Junonia almana* are available under NCBI BioProject PRJNA1300591. Lists of differentially expressed genes and enriched Gene Ontology terms generated in the transcriptomic analysis and lists of HCR probe sequences are available via figshare at https://doi.org/10.6084/m9.figshare.c.8026060.v1 (ref. 55). Source data are provided with this paper.

References

1. West-Eberhard, M. J. Phenotypic plasticity and the origins of diversity. *Annu. Rev. Ecol. Syst.* **20**, 249–278 (1989).
2. Stearns, S. C. The evolutionary significance of phenotypic plasticity. *Bioscience* **39**, 436–445 (1989).
3. Pfennig, D. W. et al. Phenotypic plasticity's impacts on diversification and speciation. *Trends Ecol. Evol.* **25**, 459–467 (2010).
4. Tian, S. & Monteiro, A. A transcriptomic atlas underlying developmental plasticity of seasonal forms of Bicyclus anynana butterflies. *Mol. Biol. Evol.* **39**, msac126 (2022).
5. Qiu, B. et al. Canalized gene expression during development mediates caste differentiation in ants. *Nat. Ecol. Evol.* **6**, 1753–1765 (2022).
6. Casasa, S., Zattara, E. E. & Moczek, A. P. Nutrition-responsive gene expression and the developmental evolution of insect polyphenism. *Nat. Ecol. Evol.* **4**, 970–978 (2020).
7. Lafuente, E., Duneau, D. & Beldade, P. Genetic basis of thermal plasticity variation in *Drosophila melanogaster* body size. *PLoS Genet.* **14**, e1007686 (2018).
8. Lafuente, E. & Beldade, P. Genomics of developmental plasticity in animals. *Front. Genet.* **10**, 720 (2019).
9. van der Burg, K. R. et al. Genomic architecture of a genetically assimilated seasonal color pattern. *Science* **370**, 721–725 (2020).
10. Lafuente, E., Duneau, D. & Beldade, P. Genetic basis of variation in thermal developmental plasticity for *Drosophila melanogaster* body pigmentation. *Mol. Ecol.* **33**, e17294 (2024).
11. Brakefield, P. M. & Reitsma, N. Phenotypic plasticity, seasonal climate and the population biology of *Bicyclus* butterflies (Satyridae) in Malawi. *Ecol. Entomol.* **16**, 291–303 (1991).
12. Brakefield, P. M. & Larsen, T. B. The evolutionary significance of dry and wet season forms in some tropical butterflies. *Biol. J. Linn. Soc.* **22**, 1–12 (1984).
13. Lyytinen, A., Brakefield, P. M., Lindström, L. & Mappes, J. Does predation maintain eyespot plasticity in *Bicyclus anynana*?. *Proc. R. Soc. Lond. Ser. B Biol. Sci.* **271**, 279–283 (2004).
14. Prudic, K. L., Stoehr, A. M., Wasik, B. R. & Monteiro, A. Eyespots deflect predator attack increasing fitness and promoting the evolution of phenotypic plasticity. *Proc. R. Soc. B Biol. Sci.* **282**, 20141531 (2015).
15. Oostra, V., Brakefield, P. M., Hiltemann, Y., Zwaan, B. J. & Brattström, O. On the fate of seasonally plastic traits in a rainforest butterfly under relaxed selection. *Ecol. Evol.* **4**, 2654–2667 (2014).
16. van Bergen, E. et al. Conserved patterns of integrated developmental plasticity in a group of polyphenic tropical butterflies. *BMC Evol. Biol.* **17**, 1–13 (2017).
17. Bhardwaj, S. et al. Origin of the mechanism of phenotypic plasticity in satyrid butterfly eyespots. *Elife* **9**, e49544 (2020).
18. Molleman, F. et al. Larval growth rate is not a major determinant of adult wing shape and eyespot size in the seasonally polyphenic butterfly *Melanitis leda*. *PeerJ* **12**, e18295 (2024).
19. Peña, C. et al. Higher level phylogeny of Satyrinae butterflies (Lepidoptera: Nymphalidae) based on DNA sequence data. *Mol. Phylogenet. Evol.* **40**, 29–49 (2006).
20. Chazot, N. et al. Conserved ancestral tropical niche but different continental histories explain the latitudinal diversity gradient in brush-footed butterflies. *Nat. Commun.* **12**, 5717 (2021).
21. Oostra, V. et al. Translating environmental gradients into discontinuous reaction norms via hormone signalling in a polyphenic butterfly. *Proc. R. Soc. B Biol. Sci.* **278**, 789–797 (2011).
22. Mateus, A. R. A. et al. Adaptive developmental plasticity: compartmentalized responses to environmental cues and to corresponding internal signals provide phenotypic flexibility. *BMC Biol.* **12**, 1–15 (2014).
23. Monteiro, A. et al. Differential expression of ecdysone receptor leads to variation in phenotypic plasticity across serial homologs. *PLoS Genet.* **11**, e1005529 (2015).

24. Kooi, R. E. & Brakefield, P. M. The critical period for wing pattern induction in the polyphenic tropical butterfly *Bicyclus anynana* (Satyrinae). *J. Insect Physiol.* **45**, 201–212 (1999).
25. Beldade, P. & Monteiro, A. Eco-evo-devo advances with butterfly eyespots. *Curr. Opin. Genet. Dev.* **69**, 6–13 (2021).
26. Matsuoka, Y. & Monteiro, A. Hox genes are essential for the development of eyespots in *Bicyclus anynana* butterflies. *Genetics* **217**, iyaa005 (2021).
27. Banerjee, T. D. & Monteiro, A. Reuse of an insect wing venation gene-regulatory subnetwork in patterning the eyespot rings of butterflies. Preprint at *bioRxiv* https://doi.org/10.1101/2021.05.22.445259 (2023).
28. Saenko, S. V., Marialva, M. S. & Beldade, P. Involvement of the conserved Hox gene *Antennapedia* in the development and evolution of a novel trait. *EvoDevo* **2**, 1–10 (2011).
29. Shirai, L. T. et al. Evolutionary history of the recruitment of conserved developmental genes in association to the formation and diversification of a novel trait. *BMC Evol. Biol.* **12**, 1–11 (2012).
30. Oliver, J. C., Tong, X.-L., Gall, L. F., Piel, W. H. & Monteiro, A. A single origin for nymphalid butterfly eyespots followed by widespread loss of associated gene expression. *PLoS Genet.* **8**, e1002893 (2012).
31. Matsuoka, Y., Murugesan, S. N., Prakash, A. & Monteiro, A. Lepidopteran prolegs are novel traits, not leg homologs. *Sci. Adv.* **9**, eadd9389 (2023).
32. Murugesan, S. N. et al. Butterfly eyespots evolved via cooption of an ancestral gene-regulatory network that also patterns antennae, legs, and wings. *Proc. Natl Acad. Sci. USA* **119**, e2108661119 (2022).
33. Saleh Ziabari, O. et al. Gene duplication captures morph-specific promoter usage in the evolution of aphid wing dimorphisms. *Proc. Natl Acad. Sci. USA* **122**, e2420893122 (2025).
34. Demircioğlu, D. et al. A pan-cancer transcriptome analysis reveals pervasive regulation through alternative promoters. *Cell* **178**, 1465–1477 (2019).
35. Saccheri, I. J. et al. The genome sequence of the squinting bush brown, *Bicyclus anynana* (Butler, 1879). *Wellcome Open Res.* **8**, 280 (2023).
36. Phan, M. H. et al. Conservation of regulatory elements with highly diverged sequences across large evolutionary distances. *Nat. Genet.* **57**, 1524–1534 (2025).
37. Tendolkar, A. et al. Cis-regulatory modes of *Ultrabithorax* inactivation in butterfly forewings. *ELife* **12**, RP90846 (2024).
38. Andersson, R. & Sandelin, A. Determinants of enhancer and promoter activities of regulatory elements. *Nat. Rev. Genet.* **21**, 71–87 (2020).
39. Jin, V. X., Singer, G. A., Agosto-Pérez, F. J., Liyanarachchi, S. & Davuluri, R. V. Genome-wide analysis of core promoter elements from conserved human and mouse orthologous pairs. *BMC Bioinf.* **7**, 114 (2006).
40. Haberle, V. & Stark, A. Eukaryotic core promoters and the functional basis of transcription initiation. *Nat. Rev. Mol. Cell Biol.* **19**, 621–637 (2018).
41. Özsu, N., Chan, Q. Y., Chen, B., Gupta, M. D. & Monteiro, A. Wingless is a positive regulator of eyespot color patterns in *Bicyclus anynana* butterflies. *Dev. Biol.* **429**, 177–185 (2017).
42. Banerjee, T. D., Shan, S. K. & Monteiro, A. Optix is involved in eyespot development via a possible positional information mechanism. Preprint at *bioRxiv* https://doi.org/10.1101/2021.05.22.445259 (2023).
43. Peña, C. & Wahlberg, N. Prehistorical climate change increased diversification of a group of butterflies. *Biol. Lett.* **4**, 274–278 (2008).
44. Halali, S., Brakefield, P. M. & Brattström, O. Phenotypic plasticity in tropical butterflies is linked to climatic seasonality on a macroevolutionary scale. *Evolution* **78**, 1302–1316 (2024).
45. Gompel, N., Prud'homme, B., Wittkopp, P. J., Kassner, V. A. & Carroll, S. B. Chance caught on the wing: cis-regulatory evolution and the origin of pigment patterns in *Drosophila*. *Nature* **433**, 481–487 (2005).
46. Chan, Y. F. et al. Adaptive evolution of pelvic reduction in sticklebacks by recurrent deletion of a Pitx1 enhancer. *Science* **327**, 302–305 (2010).
47. Kvon, E. Z. et al. Progressive loss of function in a limb enhancer during snake evolution. *Cell* **167**, 633–642. e611 (2016).
48. Mazo-Vargas, A. et al. Deep cis-regulatory homology of the butterfly wing pattern ground plan. *Science* **378**, 304–308 (2022).
49. Moreno, J. A. et al. Emx2 underlies the development and evolution of marsupial gliding membranes. *Nature* **629**, 127–135 (2024).
50. Shahandeh, M. P. et al. Circadian plasticity evolves through regulatory changes in a neuropeptide gene. *Nature* **635**, 951–959 (2024).
51. Galupa, R. et al. Enhancer architecture and chromatin accessibility constrain phenotypic space during *Drosophila* development. *Dev. Cell* **58**, 51–62. e54 (2023).
52. McDonald, J. M. & Reed, R. D. Beyond modular enhancers: new questions in cis-regulatory evolution. *Trends Ecol. Evol.* **39**, 1035–1046 (2024).
53. Murugesan, S. N. & Monteiro, A. Evolution of modular and pleiotropic enhancers. *J. Exp. Zool. Part B* **340**, 105–115 (2023).
54. Banerjee, T. D., Tian, S. & Monteiro, A. Laser microdissection-mediated isolation of butterfly wing tissue for spatial transcriptomics. *Methods Protoc.* **5**, 67 (2022).
55. Tian, S. et al. A novel Hox gene promoter fuels the evolution of adaptive phenotypic plasticity in wing eyespots of satyrid butterflies. *figshare* https://doi.org/10.6084/m9.figshare.c.8026060.v1 (2025).
56. Choi, H. M. et al. Third-generation in situ hybridization chain reaction: multiplexed, quantitative, sensitive, versatile, robust. *Development* **145**, dev165753 (2018).
57. Bruce, H. S. et al. Hybridization chain reaction (HCR) in situ protocol. *protocols.io* https://doi.org/10.17504/protocols.io.bunznvf6 (2021).
58. Banerjee, T. D., Zhang, L. & Monteiro, A. Mapping gene expression in whole larval brains of *Bicyclus anynana* butterflies. *Methods Protoc.* **8**, 31 (2025).
59. Banerjee, T. D. & Monteiro, A. CRISPR-Cas9 mediated genome editing in *Bicyclus anynana* butterflies. *Methods Protoc.* **1**, 16 (2018).
60. Murugesan, S. N., Tian, S. & Monteiro, A. Genome assembly and annotation of the dark-branded bushbrown butterfly *Mycalesis mineus* (Nymphalidae: Satyrinae). *Genome Biol. Evol.* **16**, evae051 (2024).
61. Chazot, N. et al. Conserved ancestral tropical niche but different continental histories explain the latitudinal diversity gradient in brush-footed butterflies. *Zenodo* https://doi.org/10.5281/zenodo.5463912 (2021).
62. Kumar, S. et al. TimeTree 5: an expanded resource for species divergence times. *Mol. Biol. Evol.* **39**, msac174 (2022).

Acknowledgements

We thank J. Lee for his assistance with the promoter usage analysis. We thank K. Long Tan for helping rear the promoter knockout lines. We acknowledge National Research Foundation (NRF) Singapore award NRF-CRP20-2017-0001 (A.M.), NRF Singapore award NRF-CRP25-2020-0001 (A.M.), NRF Singapore award NRF-NRFI05-2019-0006 (A.M.) and Ministry of Education Singapore award MOE-T2EP30223-0007 (A.M.).

Author contributions

Conceptualization: S.T. and A.M. Methodology: S.T., T.D.B. and A.M. Investigation: S.T., B.L., T.D.B. and S.N.M. Visualization: S.T., B.L. and

T.D.B. Funding acquisition: A.M. Project administration: S.T. and A.M. Supervision: A.M. Writing—original draft: S.T. and A.M. Writing–review and editing: S.T., T.D.B. and A.M.

Competing interests
The authors declare no competing interests.

Additional information
Extended data is available for this paper at https://doi.org/10.1038/s41559-025-02891-5.

Supplementary information The online version contains supplementary material available at https://doi.org/10.1038/s41559-025-02891-5.

Correspondence and requests for materials should be addressed to Shen Tian or Antónia Monteiro.

Peer review information *Nature Ecology & Evolution* thanks Jennifer Brisson, Sofia Casasa and the other, anonymous, reviewer(s) for their contribution to the peer review of this work. Peer reviewer reports are available.

Reprints and permissions information is available at www.nature.com/reprints.

Publisher's note Springer Nature remains neutral with regard to jurisdictional claims in published maps and institutional affiliations.

Springer Nature or its licensor (e.g. a society or other partner) holds exclusive rights to this article under a publishing agreement with the author(s) or other rightsholder(s); author self-archiving of the accepted manuscript version of this article is solely governed by the terms of such publishing agreement and applicable law.

© The Author(s), under exclusive licence to Springer Nature Limited 2025

https://doi.org/10.1038/s41559-025-02891-5

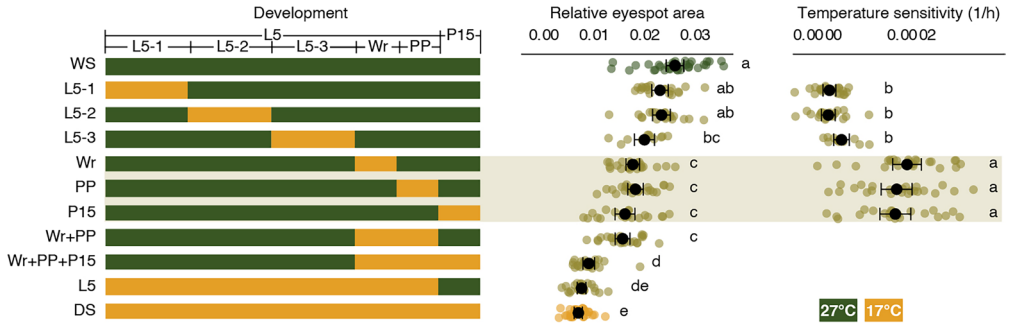

Extended Data Fig. 1 | Temperature-shift experiments identified a prolonged temperature sensitivity window. Shift schemes in refined temperature-shift experiments are illustrated (left panel). See Methods and Supplementary Table 1 for detailed methods and statistics of the temperature-shift experiments. Ventral Cu1 eyespot areas (middle panel), and temperature sensitivities (right panel, only across the six non-overlapping windows) were quantified and compared across the schemes in a one-way ANCOVA (Methods). n = 35 (WS), 20 (L5-1), 20 (L5-2), 12 (L5-3), 24 (Wr), 23 (PP), 22 (P15), 23 (Wr+PP), 23 (Wr+PP + P15), 24 (L5), 27 (DS). Black dots with error bars represent mean values ± 95CI. Eyespot areas from shift schemes with the same letter are not significantly different from each other, as determined by Tukey's test. WS, wet season; DS, dry season; L5, 5th instar larva; Wr, wanderer, PP, prepupa; P, pupa.

https://doi.org/10.1038/s41559-025-02891-5

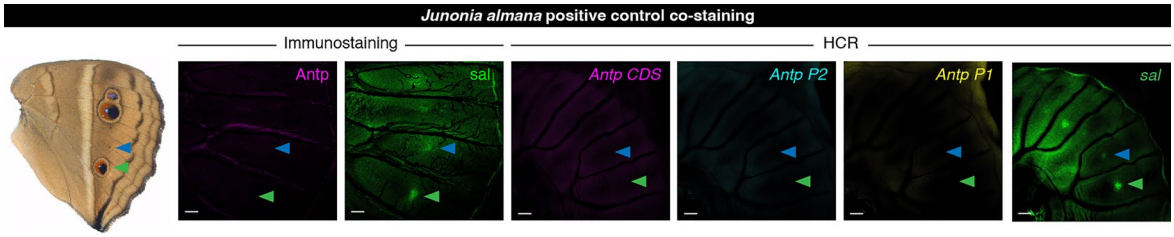

Extended Data Fig. 2 | Co-staining of a positive eyespot marker *sal* in *J. almana*. *Sal* was used as a positive eyespot marker in both immunostaining and HCR. For immunostaining and HCR, n = 3 replicates. Scale bar: 100 microns.

https://doi.org/10.1038/s41559-025-02891-5

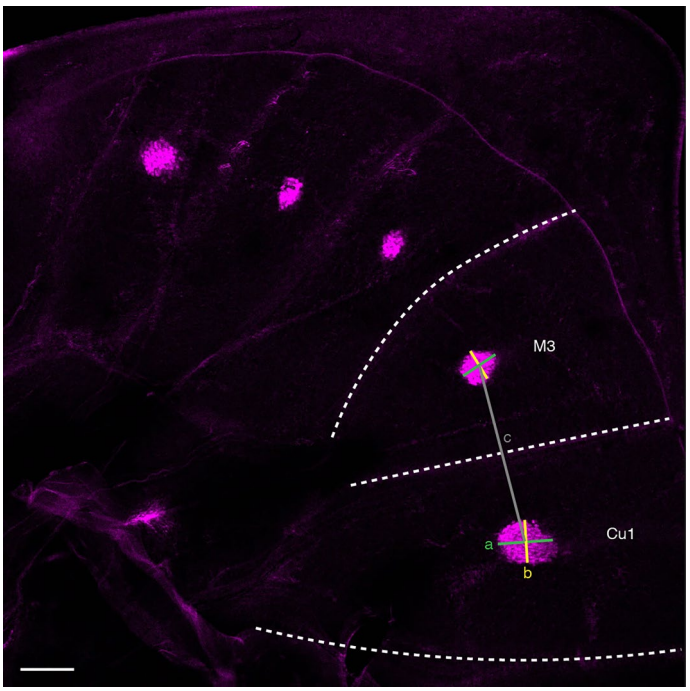

Extended Data Fig. 3 | Calculation of Antp protein eyespot expression diameter. Size of the Antp protein expression domain in eyespots was calculated as eyespot expression diameter. For each ventral hindwing eyespot (here we use Cu1 eyespot as an example), eyespot expression diameter was calculated as the mean of the two diameters of the Antp protein expression domain (**a** and **b**), one (**a**) was parallel to the proximal-distal axis of the sector (outlined in dotted lines), while the other (**b**) perpendicular to it. The distance between M3 and Cu1 eyespot centers (**c**) was constantly used as a hindwing size proxy, and entered as a covariate in statistical analyses. Scale bar: 100 microns.

https://doi.org/10.1038/s41559-025-02891-5

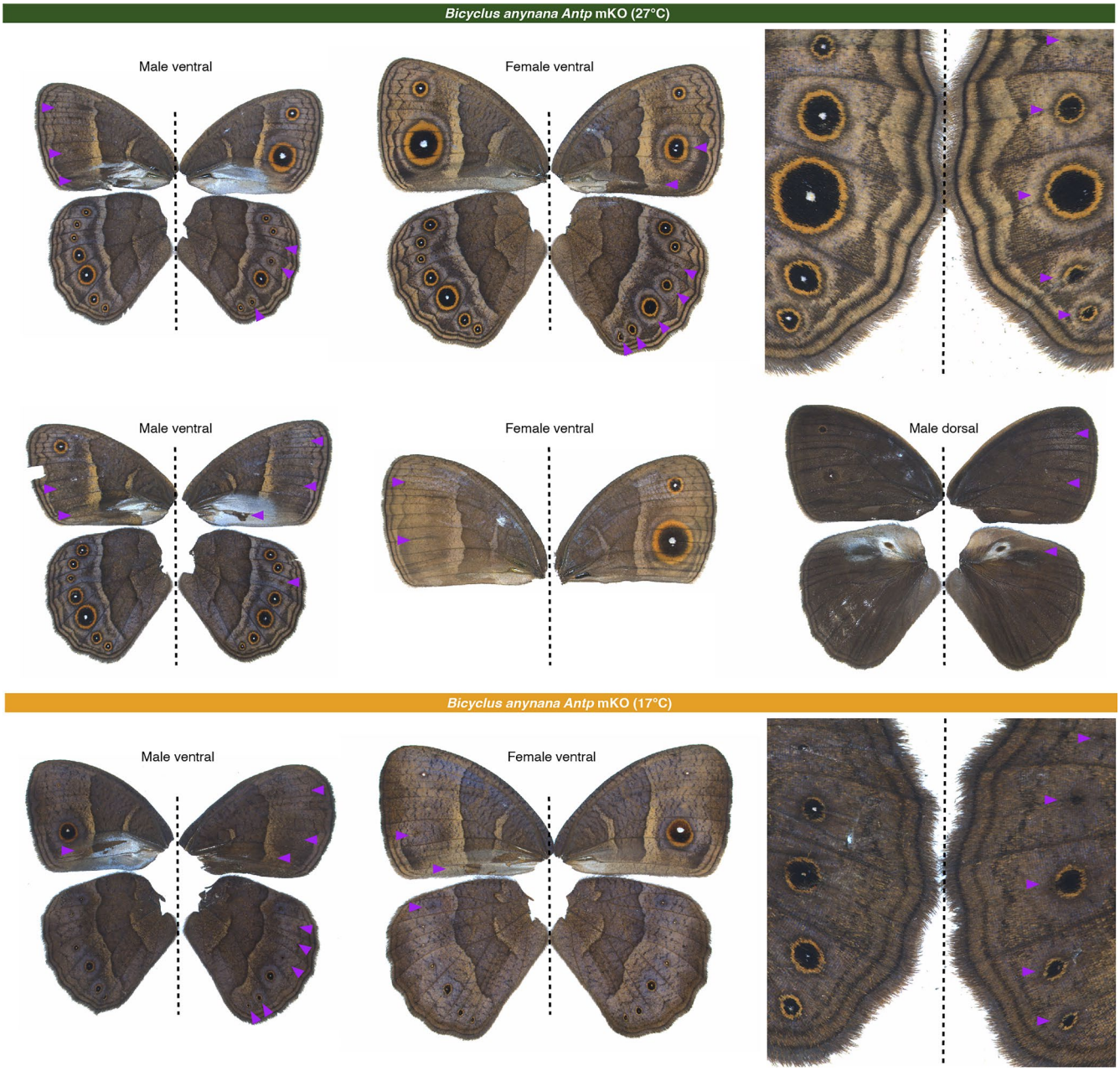

Extended Data Fig. 4 | Representative phenotypes of *Antp* mKO crispants in *B. anynana*. A dotted line separates left and right sides of the same individual. Purple arrowheads denote mutant phenotypes.

https://doi.org/10.1038/s41559-025-02891-5

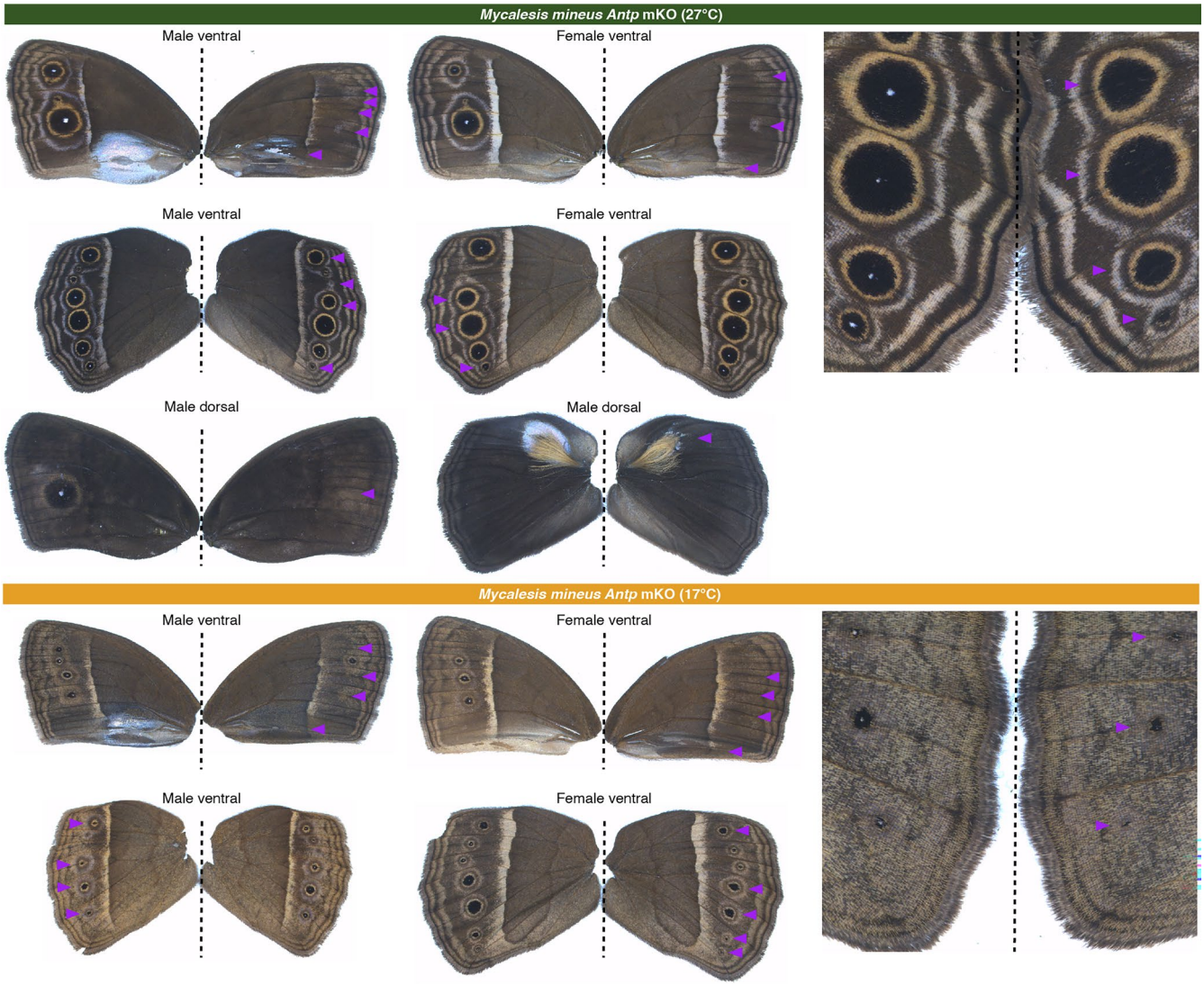

Extended Data Fig. 5 | Representative phenotypes of *Antp* mKO crispants in *M. mineus*. A dotted line separates left and right sides of the same individual. Purple arrowheads denote mutant phenotypes.

https://doi.org/10.1038/s41559-025-02891-5

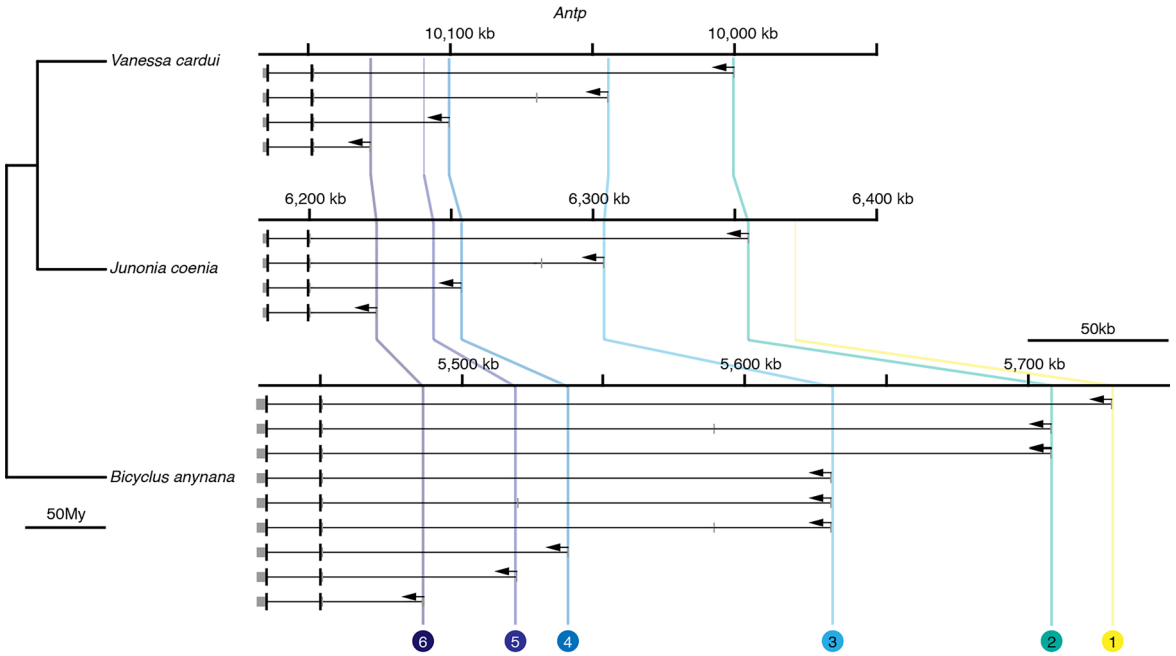

Extended Data Fig. 6 | Conservation of sequences and transcriptional activities of *Antp* promoters across *B. anynana* and two non-satyrid butterflies. *Antp* transcript annotation and sequence conservation around the six *Antp* promoter regions in *B. anynana* and two non-satyrids, *V. cardui* and *J. coenia*. Six alternative promoters are labeled. For transcripts, coding regions (CDSs) are in black and untranslated regions (UTRs) are in gray. *Antp* transcript annotation for *J. coenia* is from[37].

https://doi.org/10.1038/s41559-025-02891-5

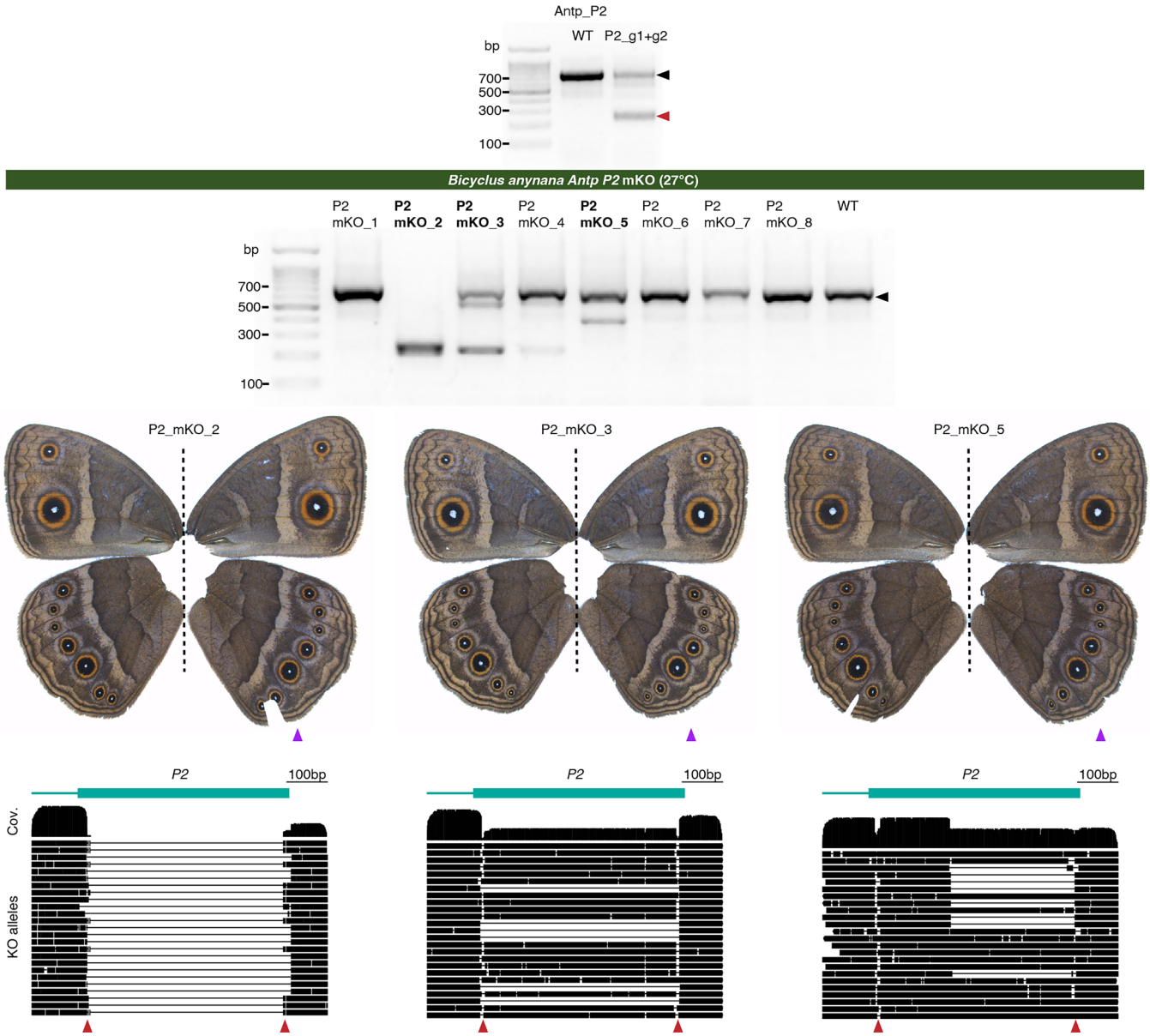

Extended Data Fig. 7 | *Antp P2* mKO crispants in *B. anynana*. Two guide RNAs co-injected efficiently induced long deletions around the conserved sequences (Fig. 4d middle panel) of *Antp P2* in vivo, confirmed in pooled injected eggs (upper panel). The WT bands and mutant bands are denoted by black and red arrowheads, respectively. Genomic DNA was extracted from right hindwings of eight mKO crispants, and subjected to PCR and gel electrophoresis to detect potential long deletions (middle panel). Three crispants showing clear long deletions were genotyped via Nanopore amplicon sequencing. A dotted line separates left and right sides of the same individual. Purple arrowheads denote the wings used for genotyping, and red arrowheads denote guide RNA cut sites. Sequence coverage (Cov.) across the amplicon and major KO alleles are shown (lower panel).

https://doi.org/10.1038/s41559-025-02891-5

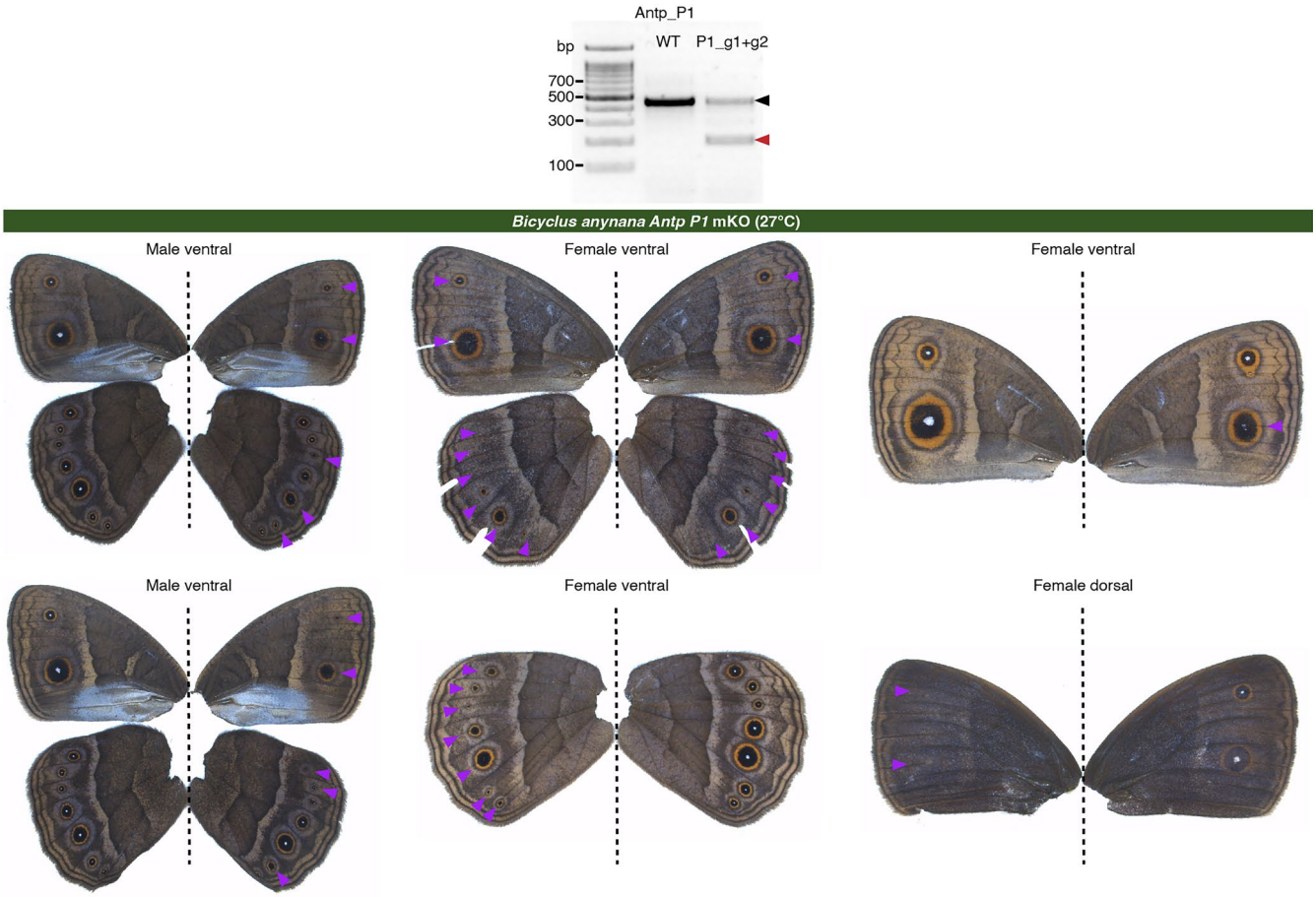

Extended Data Fig. 8 | *Antp P1* mKO crispants in *B. anynana*. Two guide RNAs co-injected efficiently induced long deletions around the conserved sequences (Fig. 4d right panel) of *Antp P1* in vivo, confirmed in pooled injected eggs (top panel). The WT bands and mutant bands are denoted by black and red arrowheads, respectively. A dotted line separates left and right sides of the same individual. Purple arrowheads denote mutant phenotypes.

https://doi.org/10.1038/s41559-025-02891-5

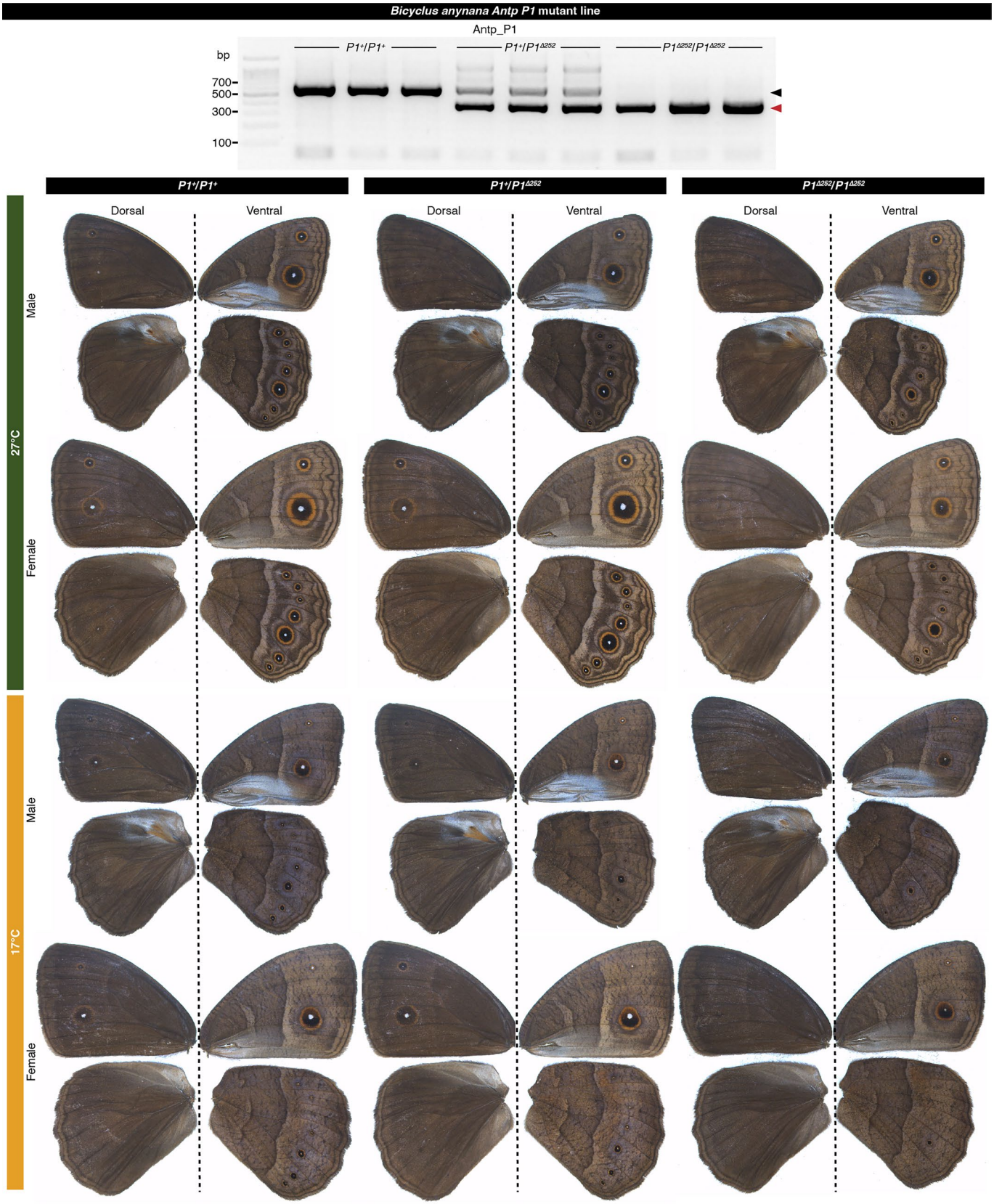

Extended Data Fig. 9 | An *Antp P1* mutant line in *B. anynana*. A mutant line carrying a 252 bp deletion around the conserved region (Fig. 4d right panel) of *Antp P1* was generated (Methods). The gel image shows clear differentiation of PCR bands across WT, mutant heterozygotes, and mutant homozygotes. The WT bands and mutant bands are denoted by black and red arrowheads, respectively. Representative wings for each genotype in both seasonal forms are shown. A dotted line separates dorsal (left) and ventral (right) sides of the same individual.

https://doi.org/10.1038/s41559-025-02891-5

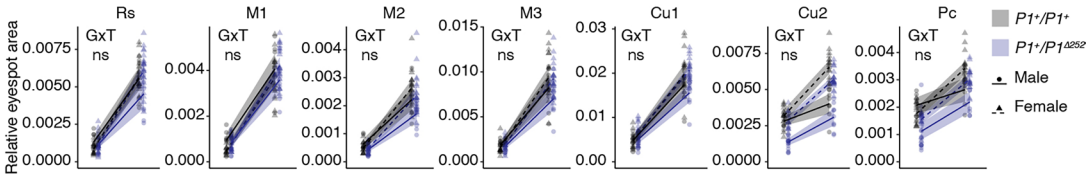

Extended Data Fig. 10 | *Antp P1* mutant heterozygotes do not exhibit significant changes in plasticity levels. Changes in eyespot size plasticity levels were assessed (two-tailed) across sib-paired WT ($P1^{+}/P1^{+}$, n = 27 (WS) and 20 (DS) individuals) and mutant heterozygotes ($P1^{+}/P1^{\Delta 252}$, n = 30 (WS) and 33 (DS) individuals) in a two-way ANCOVA, indicated by a significant (padj<0.05) genotype (G) x temperature (T) interaction (padj: 0.72 (Rs), 0.78 (M1), 0.80 (M2), 0.88 (M3), 1.0 (Cu1), 0.90 (Cu2), 0.82 (Pc)). Lines with error bands represent mean values ± 95CI. Detailed sample sizes are summarized in Supplementary Table 10. Full statistical results are summarized in Supplementary Table 11. P values were adjusted for multiple comparisons using the Benjamini-Hochberg procedure. ns, not significant; *padj<0.05; **padj<0.01; ***padj<0.001.

nature portfolio

Corresponding author(s): Shen Tian, Antonia Monteiro

Last updated by author(s): Sep 13, 2025

Reporting Summary

Nature Portfolio wishes to improve the reproducibility of the work that we publish. This form provides structure for consistency and transparency in reporting. For further information on Nature Portfolio policies, see our Editorial Policies and the Editorial Policy Checklist.

Statistics

For all statistical analyses, confirm that the following items are present in the figure legend, table legend, main text, or Methods section.

n/a	Confirmed	
☐	☒	The exact sample size (*n*) for each experimental group/condition, given as a discrete number and unit of measurement
☐	☒	A statement on whether measurements were taken from distinct samples or whether the same sample was measured repeatedly
☐	☒	The statistical test(s) used AND whether they are one- or two-sided *Only common tests should be described solely by name; describe more complex techniques in the Methods section.*
☐	☒	A description of all covariates tested
☐	☒	A description of any assumptions or corrections, such as tests of normality and adjustment for multiple comparisons
☐	☒	A full description of the statistical parameters including central tendency (e.g. means) or other basic estimates (e.g. regression coefficient) AND variation (e.g. standard deviation) or associated estimates of uncertainty (e.g. confidence intervals)
☐	☒	For null hypothesis testing, the test statistic (e.g. *F*, *t*, *r*) with confidence intervals, effect sizes, degrees of freedom and *P* value noted *Give P values as exact values whenever suitable.*
☒	☐	For Bayesian analysis, information on the choice of priors and Markov chain Monte Carlo settings
☒	☐	For hierarchical and complex designs, identification of the appropriate level for tests and full reporting of outcomes
☒	☐	Estimates of effect sizes (e.g. Cohen's *d*, Pearson's *r*), indicating how they were calculated

Our web collection on statistics for biologists contains articles on many of the points above.

Software and code

Policy information about availability of computer code

Data collection	Software used to measure the size of eyespot/wing/Antp expression domain: Adobe Photoshop 2021.
Data analysis	Software used for: RNA-seq adapter trimming: Trimmomatic 0.39 RNA-seq sequence alignment: Salmon 1.6.0, STAR 2.7.10a Gene expression analysis: DESeq2 1.38.3 Gene set enrichment analysis: Babelomics 5 Promoter usage analysis: proActiv 1.3.4 J. almana genome assembly: BBMap 38.96, Platanus 1.2.4 Genotyping via Sanger sequencing: Synthego ICE Analysis tool v3 Genotyping via Nonapore sequencing: minimap2 2.26, Integrated Genomics Viewer (IGV) 2.17.3 Statistical tests: R 4.2.3, car 3.1-2, rstatix 0.7.2, emmeans 1.10.7, multcomp 1.4-26

For manuscripts utilizing custom algorithms or software that are central to the research but not yet described in published literature, software must be made available to editors and reviewers. We strongly encourage code deposition in a community repository (e.g. GitHub). See the Nature Portfolio guidelines for submitting code & software for further information.

Data

Policy information about availability of data

All manuscripts must include a data availability statement. This statement should provide the following information, where applicable:

- Accession codes, unique identifiers, or web links for publicly available datasets
- A description of any restrictions on data availability
- For clinical datasets or third party data, please ensure that the statement adheres to our policy

All data required for reproducing and extending the study are available in the main text or the supplementary materials. Raw RNA-seq data for Bicyclus anynana are available under NCBI BioProject PRJNA1268022. Raw genome sequencing and assembly data for Junonia almana are available under NCBI BioProject PRJNA1300591. Lists of differentially expressed genes and enriched Gene Ontology terms generated in the transcriptomic analysis, and lists of HCR probe sequences, are available in a Figshare repository (doi.org/10.6084/m9.figshare.c.8026060.v1). Source data are provided with this paper.

Research involving human participants, their data, or biological material

Policy information about studies with human participants or human data. See also policy information about sex, gender (identity/presentation), and sexual orientation and race, ethnicity and racism.

Reporting on sex and gender	n/a
Reporting on race, ethnicity, or other socially relevant groupings	n/a
Population characteristics	n/a
Recruitment	n/a
Ethics oversight	n/a

Note that full information on the approval of the study protocol must also be provided in the manuscript.

Field-specific reporting

Please select the one below that is the best fit for your research. If you are not sure, read the appropriate sections before making your selection.

☐ Life sciences ☐ Behavioural & social sciences ☒ Ecological, evolutionary & environmental sciences

For a reference copy of the document with all sections, see nature.com/documents/nr-reporting-summary-flat.pdf

Ecological, evolutionary & environmental sciences study design

All studies must disclose on these points even when the disclosure is negative.

Study description

This study consists of multiple experimental units, major experimental units involving collecting/genanerating quantitative data are described below:

1. Temperature shift experiments included rearing B. anynana females across a series of temperature shift schemes and quantifying eyespot size across the schemes. Eyespot size quantification included at least 20 females in each scheme, except for L5-3, where 12 females were used (Supplementary Table 1). Eyespot size and its temperature sensitivity were compared across the schemes, where hindwing size was entered as a covariate in a one-way ANCOVA.

2. Spatial transcriptomic profiling via laser-microdissection sampled and pooled 30 hindwings (both sides) from 15 B. anynana female larvae, or 8 hindwings (one side) from 8 female pupae, as one biological replicate. Four biological replicates were included in each seasonal form and developmental stage.

3. Gene expression and functional enrichment analysis were performed using the newly generated spatial transcriptomic data. Promoter usage analysis integrated both the new data and a series of published tissue/body part-specific transcriptomic data (Matsuoka et al. 2023, Murugesan et al. 2022). All included 4 biological replicates in each condition.

4. After Antp immonostaining, eyespot expression diameter of Antp protein was quantified across seasonal forms of B. anynana and M. mineus female larval wings. Wings from 14 DS and 13 WS B. anynana females, or from 7 DS and 13 WS M. mineus females, were included. Eyespot expression diameter was quantified and compared across seasonal forms in each eyespot, where a hindwing size proxy was entered as a covariate in a one-way ANCOVA.

5. Mosaic Antp KO crispants of B. anynana and M. mineus were manually inspected for the presence or absence of the white eyespot center to assign the eyespots either as WT or KO. Mosaic crispants with paired phenotypes (eyespots from one side assigned as WT

and the other as KO) were scored as many as possible and the sample size for each combination of hindwing eyespot/genotype/seasonal form/sex/species was summarized in Supplementary Table 7. Eyespot size was quantified and responses of eyespot size to temperatures across WT and KO eyespots were assessed in each species, where genotype and temperature were entered as interacting factors, with hindwing size and sex entered as covariates, in a two-way ANCOVA.

6. Eyespot size from sib-paired WT, mutant heterozygotes, and mutant homozygotes of a Antp P1 KO line was quantified across seasonal forms. Sib-paired individuals were quantified as many as possible and the sample size for each combination of hindwing eyespot/genotype/seasonal form/sex was summarized in Supplementary Table 10. Eyespot size was quantified and responses of eyespot size to temperatures across WT and mutant heterozygotes, or across WT and mutant homozygotes, were assessed, where genotype and temperature were entered as interacting factors, with hindwing size and sex entered as covariates, in a two-way ANCOVA.

Research sample

This study involved two satyrid species, B. anynana and M. mineus, and one outgroup non-satyrid species, J. almana. Lab populations of B. anynana butterflies have been reared in the laboratory since 1988, originally collected in Malawi. M. mineus and J. almana were collected from Singapore.

Sampling strategy

No sample size calculation was performed. The choice of sample size was based on previous studies with similar data types (temperature shift experiments, quantification of eyespot expression domain of Antp protein), or the maximum sample size possible:

To quantify eyespot size across Antp mosaic KO crispants, we tried to obtain as many mosaic crispants as possible by injecting over 2700 eggs in B. anynana, and over 3800 eggs in M. mineus (Supplementary Table 4), and we obtained a sample size that was sufficient to perform statistical analysis (Supplementary Table 7).

To quantify eyespot size across the Antp P1 mutant genotypes, we sampled all the sib-paired F2 offsprings from the F1 heterozygous parents that survived till adulthood, and we obtained a sample size that was sufficient to perform statistical analysis (Supplementary Table 10)

Data collection

ST collected wing tissues and performed measurements on eyespot size/eyespot expression diameter of Antp protein for the temperature shift experiments and immunostaining. ST collected samples, and TDB performed laser-microdissection. ST performed CRSPR-mediated Antp KO experiments, collected and scored wings from mosaic crispants, and performed eyespot size measurements. SNM collected J. almana and extracted genomic DNA for genome assembly. BL collected and genotyped Antp P1 mutant F2 individuals, imaged the wings, and ST performed eyespot size measurements.

Timing and spatial scale

Lab populations of B. anynana butterflies have been reared in the laboratory since 1988, originally collected in Malawi. M. mineus butterflies were collected from Clementi Forest, Singapore, in August 2023, J. almana butterflies were collected from Seletar West Farmway, Singapore, in June 2024. Both were maintained as temporary lab stocks.

Data exclusions

No data were excluded from the analysis.

Reproducibility

For laser-microdissection, clean clustering of whole transcriptomic gene expression profiles among biological replicates indicates high data quality and reproducibility with minimal intragroup variations (Supplementary Fig. 1).

All the staining results (immunostainig and HCR) were replicated in at least three individuals, showing consistent expression patterns.

Randomization

For the temperature shift experiments, B. anynana females from the same lab colony were randomly assigned for different shift schemes.

For Antp immunostaining, eggs were collected from the same lab colony of B. anynana or M. mineus, and were randomly distributed in the two climate rooms, leading to the development of seasonal forms.

For the Antp mosaic KO experiments, eggs were collected and injected from the same lab colony of B. anynana or M. mineus, and were randomly distributed in the two climate rooms, leading to the development of seasonal forms.

For the Antp P1 mutant line, F2 eggs were collected from a single pair of F1 heterozygotes, and were randomly distributred in the two climate rooms, leading to the development of seasonal forms.

Blinding

For the temperature shift experiments and immunostaining, eyespot size/eyespot expression diameter of Antp protein was measured blindly, without knowledge of the treatment group they belonged to.

To quantify eyespot size from the mosaic Antp crispants in B.anynana and M. mineus, blinding was impossible, as assigning eyespots either as WT or KO depended on the manual inspection on the presence or absence of the white eyespot centers.

To quantify eyespot size across three genotypes of the B. anynana Antp P1 KO line, eyespot size was measured blindly, without knowledge of the genotypes they belonged to.

Did the study involve field work? ☒ Yes ☐ No

Field work, collection and transport

Field conditions

Field work only included collecting wild M. mineus and J. almana butterflies. It was conducted in different regions of Singapore during morning hours on sunny days.

Location	M. mineus butterflies were collected from Clementi Forest, Singapore, J. almana butterflies were collected from Seletar West Farmway, Singapore.
Access & import/export	M. mineus and J. almana butterflies were collected under a National Parks Board permit (NP/RP14-063-7a).
Disturbance	Less than 5 females of each species were collected to minimize disturbance of the local populations.

Reporting for specific materials, systems and methods

We require information from authors about some types of materials, experimental systems and methods used in many studies. Here, indicate whether each material, system or method listed is relevant to your study. If you are not sure if a list item applies to your research, read the appropriate section before selecting a response.

Materials & experimental systems

n/a	Involved in the study
☐	☒ Antibodies
☒	☐ Eukaryotic cell lines
☒	☐ Palaeontology and archaeology
☐	☒ Animals and other organisms
☒	☐ Clinical data
☒	☐ Dual use research of concern
☒	☐ Plants

Methods

n/a	Involved in the study
☒	☐ ChIP-seq
☒	☐ Flow cytometry
☒	☐ MRI-based neuroimaging

Antibodies

Antibodies used	Primary antibodies: Mouse anti-Antp 4C3 antibody, from Developmental Studies Hybridoma Bank. Guinea Pig anti-Sal GP66.1 antibody, from Oliver et al, 2012. Secondary antibodies: Alexa Fluor 555 Goat anti-Mouse (Catalog # A-21422) Alexa Fluor 488 Goat anti-Mouse (Catalog # A32723) Alexa Fluor 555 Goat anti-Guinea Pig (Catalog # A-21435)
Validation	The two primary antibodies were previously shown to be cross-reactive across broad butterfly lineages (Bhardwaj et al. 2020, Oliver et al 2012, Shirai et al. 2012, Saenko et al. 2011).

Animals and other research organisms

Policy information about studies involving animals; ARRIVE guidelines recommended for reporting animal research, and Sex and Gender in Research

Laboratory animals	Lab populations of B. anynana butterflies have been reared in the laboratory since 1988, originally collected in Malawi.
Wild animals	M. mineus butterflies were collected from Clementi Forest, Singapore, J. almana butterflies were collected from Seletar West Farmway, Singapore. Experimental animals were either maintained as a lab stock, if possible, or killed by freezing overnight at -20 C, and were never released.
Reporting on sex	The temperature shift experiments, immunostaining, and laser-microdissection involved females only. Sexing caterpillars and pupae was performed by inspecting the sex-specific marker in the abdominal segments. To quantify plasticity levels across 1) WT and Antp KO eyespots from the B. anynana and M. mineus mosaic crispants, 2) three genotypes of the B. anynana Antp P1 KO line, sex was entered as a covarient in the statistical model, and male and female data was plotted separately in the figures to illustrate sexual differences.
Field-collected samples	All the butterflies were reared in two climate rooms, at 17 C and 27 C, leading to the development of DS form and WS form, respectively. Both climate rooms have a 12:12 day: night cycle (daytime and nighttime start from 7am and 19pm, respectively), with 60% relative humidity.
Ethics oversight	M. mineus and J. almana butterflies were collected under a National Parks Board permit (NP/RP14-063-7a).

Note that full information on the approval of the study protocol must also be provided in the manuscript.

Plants

Seed stocks	n/a
Novel plant genotypes	n/a
Authentication	n/a